

# High-dimensional data segmentation in regression settings permitting heavy tails and temporal dependence

Haeran Cho<sup>1</sup>Dom Owens<sup>2</sup>

September 21, 2022

## Abstract

We propose a data segmentation methodology for the high-dimensional linear regression problem where the regression parameters are allowed to undergo multiple changes. The proposed methodology, MOSEG, proceeds in two stages where the data is first scanned for multiple change points using a moving window-based procedure, which is followed by a location refinement stage. MOSEG enjoys computational efficiency thanks to the adoption of a coarse grid in the first stage, as well as achieving theoretical consistency in estimating both the total number and the locations of the change points without requiring independence or sub-Gaussianity. In particular, it nearly matches minimax optimal rates when Gaussianity is assumed. We also propose MOSEG.MS, a multiscale extension of MOSEG which, while comparable to MOSEG in terms of computational complexity, achieves theoretical consistency for a broader parameter space that permits multiscale change points. We demonstrate good performance of the proposed methods in comparative simulation studies and also in applications to climate science and economic datasets.

*Keywords:* data segmentation, change point, high-dimensional regression, time series analysis, multiscale

## 1 Introduction

Regression modelling in high dimensions where the number of variables is as large as or even greater than the number of observations, has received great attention with the development of data collection and storage technologies, and numerous applications are found in natural and social sciences, economics, finance and genomics, to name a few. There is a mature literature on high-dimensional linear regression modelling under the sparsity assumption, see Bühlmann and van de Geer (2011) and Tibshirani (2011) for an overview. When observations

---

<sup>1</sup>School of Mathematics, University of Bristol. Email: [haeran.cho@bristol.ac.uk](mailto:haeran.cho@bristol.ac.uk).

<sup>2</sup>School of Mathematics, University of Bristol. Email: [dom.owens@bristol.ac.uk](mailto:dom.owens@bristol.ac.uk).

are collected over time in highly nonstationary environments, it is natural to allow for the linear coefficients to undergo changes. Permitting the parameters to vary over time in a piecewise constant manner, data segmentation, a.k.a. multiple change point detection, provides a conceptually simple framework for handling nonstationarity in the data.

In this paper, we consider the problem of multiple change point detection under the following model: We observe  $(Y_t, \mathbf{x}_t)$ ,  $t = 1, \dots, n$ , with  $\mathbf{x}_t = (X_{1t}, \dots, X_{pt})^\top \in \mathbb{R}^p$  where

$$Y_t = \begin{cases} \mathbf{x}_t^\top \boldsymbol{\beta}_0 + \varepsilon_t & \text{for } \theta_0 = 0 < t \leq \theta_1, \\ \mathbf{x}_t^\top \boldsymbol{\beta}_1 + \varepsilon_t & \text{for } \theta_1 < t \leq \theta_2, \\ \vdots & \\ \mathbf{x}_t^\top \boldsymbol{\beta}_q + \varepsilon_t & \text{for } \theta_q < t \leq n = \theta_{q+1}. \end{cases} \quad (1)$$

Here,  $\{\varepsilon_t\}_{t=1}^n$  denotes a sequence of errors satisfying  $E(\varepsilon_t) = 0$  and  $\text{Var}(\varepsilon) = \sigma_\varepsilon^2 \in (0, \infty)$  for all  $t$ , which may be serially correlated. At each change point  $\theta_j$ , the vector of parameters undergoes a shift such that  $\boldsymbol{\beta}_{j-1} \neq \boldsymbol{\beta}_j$  for all  $j = 1, \dots, q$ . Then, our aim is to estimate the set of change points  $\Theta = \{\theta_j, 1 \leq j \leq q\}$  by estimating both the total number and the locations of the change points.

The data segmentation problem under (1) is considered by Bai and Perron (1998), Qu and Perron (2007) and Kirch and Reckrühm (2022), among others, when the dimension  $p$  is fixed. In high-dimensional settings, when there exists at most one change point, Lee et al. (2016) and Kaul et al. (2019b) consider the problem of detecting and locating the change point, respectively. For the general case with unknown  $q$ , several data segmentation methods exist which adopt dynamic programming (Leonardi and Bühlmann, 2016; Rinaldo et al., 2021; Xu et al., 2022), fused Lasso (Wang et al., 2022; Bai and Safikhani, 2022) or wild binary segmentation (Wang et al., 2021) algorithms for the detection of multiple change points, and Bayesian approaches also exist (Datta et al., 2019). A related yet distinct problem of testing for the presence of a single change point under the regression model has been considered in Wang and Zhao (2022) and Liu et al. (2022), and Gao and Wang (2022) consider the case where the vector of the change itself is sparse without requiring the sparsity of  $\boldsymbol{\beta}_j$ .

Against the above literature background, we list the contributions made in this paper by proposing computationally and statistically efficient data segmentation methods.

- (i) **Computational efficiency.** In data segmentation methods proposed under (1), often the computational bottleneck is the local estimation of the regression parameters via penalised  $M$ -estimation. We propose MOSEG, a moving window-based two-stage methodology where its first stage scans for multiple change points in the data using a moving window of length  $G$  on a *coarse* grid  $\{G + m[rG], m = 0, 1, \dots, \}$  with some  $r \in (0, 1)$ , which contributes greatly to the reduction of Lasso estimation steps. It is followed by a simple and computationally cheap step which improves the localisation

performance, which brings the computational complexity of the combined methodology to  $O(n/(rG) \cdot \text{Lasso}(n, p))$ .

- (ii) **Multiscale change point detection.** We propose a multiscale extension of the single-bandwidth methodology MOSEG. Referred to as MOSEG.MS, it is fully adaptive to the difficult scenarios with *multiscale* change points, where large frequent changes and small changes over long stretches of stationarity are simultaneously present, while still enjoying computational competitiveness. To the best of our knowledge, MOSEG.MS is the first data segmentation methodology under (1) that achieves detection and localisation consistency for a parameter space which permits multiscale change points and consequently, is much broader than that commonly adopted in the literature. Also, while there exist several data segmentation methods that propose to apply moving window-based procedures with multiple bandwidths, MOSEG.MS is the first attempt at such an extension in high dimensions with a guaranteed rate of localisation.
- (iii) **Theoretical consistency in general settings.** We show the consistency of MOSEG and MOSEG.MS in estimating the total number and the locations of multiple change points. Under Gaussianity, their separation and localisation rates nearly match the minimax lower bounds. Moreover, in our theoretical investigation, we permit temporal dependence as well as tail behaviour heavier than sub-Gaussianity. This, compared to the existing literature where independence and (sub-)Gaussianity assumptions are commonly made, shows that the proposed methods work well in situations that are more realistic for empirical applications.

The rest of the paper is organised as follows. Section 2 introduces MOSEG, the single-bandwidth methodology, and establishes its theoretical consistency. Then in Section 3, we propose its multiscale extension, MOSEG.MS, and show that it achieves theoretical consistency in a broad parameter space. Numerical experiments in Section 4 demonstrate the competitiveness of the proposed methods in comparison with the existing data segmentation algorithms and Section 5 provide real data applications in sea ice extent analysis and equity premium modelling. In the Appendix, we provide a comprehensive comparison between the existing methods and MOSEG and MOSEG.MS both on their theoretical and computational properties, and present all the proofs and additional numerical results. The R software implementing MOSEG and MOSEG.MS is available from <https://github.com/Dom-Owens-UoB/moseg>.

**Notation.** For a random variable  $X$ , we write  $\|X\|_\nu = [\mathbb{E}(|X|^\nu)]^{1/\nu}$  for  $\nu > 0$ . For  $\mathbf{a} = (a_1, \dots, a_p)^\top \in \mathbb{R}^p$ , we write  $\text{supp}(\mathbf{a}) = \{i, 1 \leq i \leq p : a_i \neq 0\}$ ,  $|\mathbf{a}|_0 = \sum_{i=1}^p \mathbb{I}_{\{a_i \neq 0\}}$ ,  $|\mathbf{a}|_1 = \sum_{i=1}^p |a_i|$ ,  $|\mathbf{a}|_2 = (\sum_{i=1}^p a_i^2)^{1/2}$  and  $|\mathbf{a}|_\infty = \max_{1 \leq i \leq p} |a_i|$ . For a square matrix  $\mathbf{A}$ , let  $\Lambda_{\max}(\mathbf{A})$  and  $\Lambda_{\min}(\mathbf{A})$  denote its maximum and minimum eigenvalues, respectively. For a set  $\mathcal{A}$ , we denote its cardinality by  $|\mathcal{A}|$ . For sequences of positive numbers  $\{a_n\}$  and  $\{b_n\}$ , we

write  $a_n \lesssim b_n$  if there exists some constant  $C > 0$  such that  $a_n/b_n \leq C$  as  $n \rightarrow \infty$ . Finally, we write  $a \vee b = \max(a, b)$  and  $a \wedge b = \min(a, b)$ .

## 2 Single-bandwidth methodology

We introduce MOSEG, a single-bandwidth two-stage methodology for data segmentation in regression settings. We first describe its two stages in Section 2.1, establish its theoretical consistency in Section 2.2 and verify key assumptions made for the theoretical analysis in Section 2.3 for a class of linear processes with serial dependence and heavier tails than that permitted under sub-Gaussianity.

### 2.1 MOSEG

#### 2.1.1 Stage 1: Moving window procedure on a coarse grid

Moving window procedures have successfully been adopted for data segmentation in a variety of change point problems (Preuss et al., 2015; Yau and Zhao, 2016; Eichinger and Kirch, 2018; Cho et al., 2022). We propose to detect change points under the piecewise stationary regression model in (1), by scanning the data for multiple change points using a moving window in combination with a detector statistic designed to have good detection power.

For a given bandwidth  $G \in \mathbb{N}$  satisfying  $G \leq n/2$ , our proposed detector statistic is

$$T_k(G) = \sqrt{\frac{G}{2}} \left| \hat{\beta}_{k,k+G} - \hat{\beta}_{k-G,k} \right|_2, \quad G \leq k \leq n - G. \quad (2)$$

Here,  $\hat{\beta}_{s,e}$  denotes an estimator of the vector of parameters obtained from  $(Y_t, \mathbf{x}_t)$ ,  $s+1 \leq t \leq e$ , for any  $0 \leq s < e \leq n$ . Then,  $T_k(G)$  contrasts the local parameter estimators from two adjacent data sections over  $\{k-G+1, \dots, k\}$  and  $\{k+1, \dots, k+G\}$ . By construction,  $T_k(G)$  is expected to form local maxima near the change points, provided that the local estimators are sufficiently close to their population counterparts, and thus it is well-suited for detecting and locating the change points.

Penalised  $M$ -estimators such as the Lasso (Tibshirani, 1996) have popularly been adopted for handling high dimensionality. We propose to obtain the local estimator  $\hat{\beta}_{s,e}$  as

$$\hat{\beta}_{s,e}(\lambda) = \arg \min_{\beta \in \mathbb{R}^p} \sum_{t=s+1}^e (Y_t - \mathbf{x}_t^\top \beta)^2 + \lambda \sqrt{e-s} |\beta|_1 \quad (3)$$

for some tuning parameter  $\lambda > 0$ . In what follows, we suppress the dependence of this estimator on  $\lambda$  when there is no confusion. The estimand of  $\hat{\beta}_{k-G,k}$  is a weighted sum of  $\beta_j$  with the weights corresponding to the proportion of the intervals  $\{k-G+1, \dots, k\}$  overlapping

with  $\{\theta_j + 1, \dots, \theta_{j+1}\}$ , i.e.

$$\beta_{k-G,k}^* = \frac{1}{G} \sum_{j=L(k-G+1)}^{L(k)} \{(\theta_{j+1} \wedge k) - ((k-G) \vee \theta_j)\} \beta_j, \quad (4)$$

where  $L(t) = \{j, 0 \leq j \leq q : \theta_j + 1 \leq t\}$  denotes the index of a change point  $\theta_j$  that is the closest to  $t$  while lying strictly to its left.

Scanning the detector statistic  $T_k(G)$  over all  $k \in \{G, \dots, n-G\}$  requires the computation of the Lasso estimator  $O(n)$  times, which poses a computational bottleneck particularly when the data sequence is very long or its dimensionality ultra high. Instead, we propose to evaluate  $T_k(G)$  on a coarser grid only for generating *pre-estimators* of the change points. Let  $\mathcal{T}$  denote the grid over which we evaluate  $T_k(G)$ , which is given by

$$\mathcal{T} = \mathcal{T}(r, G) = \left\{ t : t = G + \lfloor rG \rfloor m, 0 \leq m \leq \left\lfloor \frac{n-2G}{rG} \right\rfloor \right\} \quad (5)$$

with some constant  $r \in [G^{-1}, 1)$  that controls the coarseness of the grid. When  $r = G^{-1}$ , we have the finest grid  $\mathcal{T} = \{G, \dots, n-G\}$  and the grid becomes coarser with increasing  $r$ .

Motivated by Eichinger and Kirch (2018), who considered the problem of detecting multiple shifts in the mean of univariate time series using a moving window procedure, we propose to accept all significant local maximisers of  $T_k(G)$  over  $k \in \mathcal{T}$  as the pre-estimators of the change points. That is, for some threshold  $D > 0$  and  $\eta \in (0, 1]$ , we accept all  $\tilde{\theta} \in \mathcal{T}$  that simultaneously satisfy

$$T_{\tilde{\theta}}(G) > D \quad \text{and} \quad \tilde{\theta} = \arg \max_{k \in \{\tilde{\theta} - \lfloor \eta G \rfloor + 1, \dots, \tilde{\theta} + \lfloor \eta G \rfloor\} \cap \mathcal{T}} T_k(G). \quad (6)$$

We denote the set collecting all such pre-estimators by  $\tilde{\Theta} = \{\tilde{\theta}_j, 1 \leq j \leq \hat{q} : \tilde{\theta}_1 < \dots < \tilde{\theta}_{\hat{q}}\}$  with  $\hat{q} = |\tilde{\Theta}|$  as the estimator of the number of change points. This grid-based approach substantially reduces the computational complexity by requiring the Lasso estimators to be computed only  $O(n/\lfloor rG \rfloor)$  times. Even so, it is sufficient for detecting the presence of all  $q$  change points, provided that  $r$  is chosen not too large (see Theorem 1 (i) below).

### 2.1.2 Stage 2: Location refinement

Once the set of pre-estimators  $\tilde{\Theta}$  is generated by the first-stage moving window procedure on a coarse grid, we further refine the location estimators by a simple step. It involves the local evaluation and minimisation of the following objective function

$$Q(k; a, b, \hat{\gamma}^L, \hat{\gamma}^R) = \sum_{t=a+1}^k (Y_t - \mathbf{x}_t^\top \hat{\gamma}^L)^2 + \sum_{t=k+1}^b (Y_t - \mathbf{x}_t^\top \hat{\gamma}^R)^2 \quad \text{for } k = a+1, \dots, b, \quad (7)$$

for suitably chosen  $a, b$ ,  $\hat{\gamma}^L$  and  $\hat{\gamma}^R$ . A similar idea has been considered for location refinement in the change point literature, see e.g. Kaul et al. (2019b) and Xu et al. (2022).

For each  $j = 1, \dots, \hat{q}$ , let  $\tilde{\theta}_j^L = \tilde{\theta}_j - \lfloor G/2 \rfloor$  and  $\tilde{\theta}_j^R = \tilde{\theta}_j + \lfloor G/2 \rfloor$ , and consider the following local parameter estimators

$$\hat{\beta}_j^L = \hat{\beta}_{0 \vee (\tilde{\theta}_j^L - G), \tilde{\theta}_j^L} \quad \text{and} \quad \hat{\beta}_j^R = \hat{\beta}_{\tilde{\theta}_j^R, (\tilde{\theta}_j^R + G) \wedge n}, \quad (8)$$

which serve as the estimators of  $\beta_{j-1}$  and  $\beta_j$ , respectively. Then in Stage 2, we propose to obtain a refined location estimator of  $\theta_j$  from its pre-estimator  $\tilde{\theta}_j$ , as

$$\hat{\theta}_j = \arg \min_{\tilde{\theta}_j - G + 1 \leq k \leq \tilde{\theta}_j + G} Q(k; \tilde{\theta}_j - G, \tilde{\theta}_j + G, \hat{\beta}_j^L, \hat{\beta}_j^R), \quad (9)$$

for all  $j = 1, \dots, \hat{q}$ . Referring to the methodology combining the two stages as MOSEG, we provide its algorithmic description in Algorithm 1 of Appendix D.

## 2.2 Consistency of MOSEG

In this section, we establish the consistency of MOSEG under a set of assumptions which specify the distributional properties of  $(\mathbf{x}_t, \varepsilon_t)$  required for our theoretical analysis.

**Assumption 1.** We assume that  $\mathbf{E}(\mathbf{x}_t) = \mathbf{0}$  and  $\mathbf{E}(\varepsilon_t) = 0$  for all  $t = 1, \dots, n$ , and that  $\text{Cov}(\mathbf{x}_t) = \Sigma_x$  has its eigenvalues bounded, i.e. there exist  $0 \leq \omega \leq \bar{\omega} < \infty$  such that

$$\omega \leq \Lambda_{\min}(\Sigma_x) \leq \Lambda_{\max}(\Sigma_x) \leq \bar{\omega}.$$

**Assumption 2** (Deviation bound). There exist fixed constants  $C_0, C_{\text{DEV}} > 0$  and some  $\rho_{n,p} \rightarrow \infty$  as  $n, p \rightarrow \infty$ , such that  $\mathbf{P}(\mathcal{D}^{(1)} \cap \mathcal{D}^{(2)}) \rightarrow 1$ , where

$$\begin{aligned} \mathcal{D}^{(1)} &= \left\{ \max_{0 \leq s < e \leq n, e-s \geq C_0 \rho_{n,p}^2} \left| \frac{1}{\sqrt{e-s}} \sum_{t=s+1}^e \varepsilon_t \mathbf{x}_t \right|_{\infty} \leq C_{\text{DEV}} \rho_{n,p} \right\}, \\ \mathcal{D}^{(2)} &= \left\{ \max_{\substack{0 \leq s < e \leq n, e-s \geq C_0 \rho_{n,p}^2 \\ |\{s+1, \dots, e\} \cap \Theta| \leq 1}} \left| \frac{1}{\sqrt{e-s}} \sum_{t=s+1}^e (Y_t - \mathbf{x}_t^\top \beta_{s,e}^*) \mathbf{x}_t \right|_{\infty} \leq C_{\text{DEV}} \rho_{n,p} \right\}. \end{aligned}$$

**Assumption 3** (Restricted strong convexity). There exist fixed constants  $C_{\text{RSC}} > 0$  and  $\tau \in [0, 1)$  such that  $\mathbf{P}(\mathcal{R}^{(1)} \cap \mathcal{R}^{(2)}) \rightarrow 1$ , where

$$\begin{aligned} \mathcal{R}^{(1)} &= \left\{ \sum_{t=s+1}^e \mathbf{a}^\top \mathbf{x}_t \mathbf{x}_t^\top \mathbf{a} \geq (e-s)\omega |\mathbf{a}|_2 - C_{\text{RSC}} \log(p)(e-s)^\tau |\mathbf{a}|_1^2 \text{ for all} \right. \\ &\quad \left. 0 \leq s < e \leq n \text{ satisfying } e-s \geq C_0 \rho_{n,p}^2 \text{ and } \mathbf{a} \in \mathbb{R}^p \right\}, \end{aligned}$$

$$\mathcal{R}^{(2)} = \left\{ \sum_{t=s+1}^e \mathbf{a}^\top \mathbf{x}_t \mathbf{x}_t^\top \mathbf{a} \leq (e-s)\bar{\omega}|\mathbf{a}|_2 + C_{\text{RSC}} \log(p)(e-s)^\tau |\mathbf{a}|_1^2 \text{ for all } \right. \\ \left. 0 \leq s < e \leq n \text{ satisfying } e-s \geq C_0 \rho_{n,p}^2 \text{ and } \mathbf{a} \in \mathbb{R}^p \right\}.$$

Assumption 1 is commonly made in the literature on high-dimensional regression and change point problems thereof. Assumptions 2 and 3 extend the deviation bound and restricted strong convexity (RSC) conditions required for high-dimensional  $M$ -estimation (van de Geer and Bühlmann, 2009; Loh and Wainwright, 2012; Negahban et al., 2012), to change point settings. In particular, as shown in Section 2.3 below, these assumptions accommodate serial dependence and heavy-tailedness in the data.

For each  $j = 0, \dots, q$ , we denote by  $\mathcal{S}_j = \text{supp}(\beta_j)$  the support of  $\beta_j$ , and by  $\mathfrak{s} = \max_{0 \leq j \leq q} |\mathcal{S}_j|$  the maximum segment-wise sparsity of the regression parameters. We make the following assumptions on the size of change  $\delta_j = |\beta_j - \beta_{j-1}|_2$  and the spacing between the neighbouring change points through imposing conditions on  $G$ .

**Assumption 4.** There exists some constant  $C_\delta > 0$  such that  $\max_{1 \leq j \leq q} \delta_j \leq C_\delta$ .

**Assumption 5.** The bandwidth  $G$  fulfils the following conditions with  $\tau$ ,  $\rho_{n,p}$  and  $\omega$  introduced in Assumptions 1, 2 and 3.

- (a)  $2G \leq \min_{1 \leq j \leq q+1} (\theta_j - \theta_{j-1})$ .
- (b) There exists a fixed constant  $C_1 > 0$  such that

$$\min_{1 \leq j \leq q} \delta_j^2 G \geq C_1 \max \left\{ \omega^{-2} \mathfrak{s} \rho_{n,p}^2, (\omega^{-1} \mathfrak{s} \log(p))^{1/(1-\tau)} \right\}.$$

Assumption 4 is a technical condition under which we focus on the more challenging regime where the size of change is allowed to tend to zero. Assumption 5 (a) relates the choice of bandwidth  $G$  to the minimum spacing between the change points. Together, (a) and (b) specify the *separation rate* that imposes a lower bound on

$$\Delta^{(1)} = \min_{1 \leq j \leq q} \delta_j^2 \cdot \min_{0 \leq j \leq q} (\theta_{j+1} - \theta_j), \quad (10)$$

for all the  $q$  change points to be detectable by MOSEG. When there are both frequent, large changes and small changes over long stretches of stationarity, the quantity  $\Delta^{(1)}$  can be small and the condition (b) of Assumption 5 may potentially be very stringent. Later in Section 3, we propose to relax this condition by introducing a multiscale extension of MOSEG.

**Theorem 1.** Suppose that Assumptions 1, 2, 3, 4 and 5 hold. Let the tuning parameters satisfy  $\lambda \geq 4C_{\text{DEV}}\rho_{n,p}$ ,  $r \in [1/G, 1/4]$ ,  $\eta \in (4r, 1]$  and

$$\frac{48\sqrt{\mathfrak{s}}\lambda}{\omega} < D < \frac{\eta}{4\sqrt{2}} \min_{1 \leq j \leq q} \delta_j \sqrt{G}. \quad (11)$$

Then on  $\mathcal{D}^{(1)} \cap \mathcal{D}^{(2)} \cap \mathcal{R}^{(1)} \cap \mathcal{R}^{(2)}$ , the following holds.

- (i) Stage 1 of MOSEG returns  $\tilde{\Theta} = \{\tilde{\theta}_j, 1 \leq j \leq \hat{q} : \tilde{\theta}_1 < \dots < \tilde{\theta}_{\hat{q}}\}$  which satisfies

$$\hat{q} = q \quad \text{and} \quad |\tilde{\theta}_j - \theta_j| \leq \frac{48\sqrt{2\mathfrak{s}G}\lambda}{\omega\delta_j} + \lfloor rG \rfloor < \left\lfloor \frac{G}{2} \right\rfloor \quad \text{for each } j = 1, \dots, q.$$

- (ii) There exists a large enough constant  $c_0 > 0$  such that Stage 2 of MOSEG returns  $\hat{\Theta} = \{\hat{\theta}_j, 1 \leq j \leq \hat{q} : \hat{\theta}_1 < \dots < \hat{\theta}_{\hat{q}}\}$  which satisfies

$$\max_{1 \leq j \leq q} \delta_j^2 |\hat{\theta}_j - \theta_j| \leq c_0 \max \left( \mathfrak{s} \rho_{n,p}^2, (\mathfrak{s} \log(p))^{\frac{1}{1-\tau}} \right).$$

Theorem 1 (i) establishes that Stage 1 of MOSEG correctly estimates the number of change points as well as identifying their locations by the pre-estimators with some accuracy. There is a trade-off between computational efficiency and theoretical consistency with respect to the choice of  $r$ . On one hand, increasing  $r$  leads to a coarser grid  $\mathcal{T}$  with its cardinality  $|\mathcal{T}| = O(n/(rG))$ , and thus reduces the computational cost. On the other, the pre-estimators lie in the grid such that the best approximation to each change point  $\theta_j$  can be as far from  $\theta_j$  as  $\lfloor rG \rfloor/2$ , which is reflected on the localisation property of the pre-estimators. The estimation rate achieved by the final estimators  $\hat{\theta}_j$  in (ii) relates the difficulty in locating each  $\theta_j$  to  $\delta_j^{-2}$ , i.e. the location estimation is more challenging when the size of change is small. Finally, we always have  $\max_{1 \leq j \leq q} \delta_j^{-2} \max(\mathfrak{s} \rho_{n,p}^2, (\mathfrak{s} \log(p))^{1/(1-\tau)}) \lesssim G$  under Assumption 4.

### 2.3 Verification of Assumptions 2 and 3

Assumptions 2 and 3 generalise the deviation bound and the RSC condition which are often found in the high-dimensional  $M$ -estimation literature, to accommodate change points, serial dependence and heavy-tailedness. Condition 1 gives instances of  $\{(\mathbf{x}_t, \varepsilon_t)\}_{t=1}^n$  that fulfil Assumptions 2 and 3 and specify the corresponding  $\rho_{n,p}$  and  $\tau$ .

**Condition 1.** Suppose that for i.i.d. random vectors  $\boldsymbol{\xi}_t = (\xi_{1t}, \dots, \xi_{p+1,t})^\top \in \mathbb{R}^{p+1}$ ,  $t \in \mathbb{Z}$ , with  $\mathbb{E}(\boldsymbol{\xi}_t) = \mathbf{0}$  and  $\text{Cov}(\boldsymbol{\xi}_t) = \mathbf{I}$ , we have

$$\begin{bmatrix} \mathbf{x}_t \\ \varepsilon_t \end{bmatrix} = \sum_{\ell=0}^{\infty} \mathbf{D}_\ell \boldsymbol{\xi}_{t-\ell} \quad \text{with} \quad \mathbf{D}_\ell = [D_{\ell,ik}, 1 \leq i, k \leq p+1] \in \mathbb{R}^{(p+1) \times (p+1)} \quad (12)$$

subject to  $\mathbb{E}(\mathbf{x}_t \varepsilon_t) = \mathbf{0}$ . Further, there exist constants  $\Xi > 0$  and  $\varsigma > 2$  such that

$$|D_{\ell,ik}| \leq C_{ik}(1+\ell)^{-\varsigma} \quad \text{with} \quad \max \left\{ \max_{1 \leq k \leq p+1} \sum_{i=1}^{p+1} C_{ik}, \max_{1 \leq i \leq p+1} \sum_{k=1}^{p+1} C_{ik} \right\} \leq \Xi \quad (13)$$

for all  $\ell \geq 0$ . Finally, we impose either of the two conditions on  $\xi_{it}$ .



(a) There exist some constants  $C_\xi > 0$  and  $\gamma \geq 0$  such that  $(\mathbf{E}(|\xi_{it}|^\nu))^{1/\nu} = \|\xi_{it}\|_\nu \leq C_\xi \nu^\gamma$  for all  $\nu \geq 1$ .

(b)  $\xi_{it} \sim_{\text{iid}} \mathcal{N}(0, 1)$ .

**Proposition 2.** Suppose that Assumptions 1 and 4 and Condition 1 hold. Then, there exist some constants  $c_1, c_2 > 0$  such that  $\mathbf{P}(\mathcal{D}^{(1)} \cap \mathcal{D}^{(2)} \cap \mathcal{R}^{(1)} \cap \mathcal{R}^{(2)}) \geq 1 - c_1(p \vee n)^{-c_2}$ , with  $\omega = \Lambda_{\min}(\Sigma_x)/2$ ,  $\bar{\omega} = 3\Lambda_{\max}(\Sigma_x)/2$ , and  $\tau$  and  $\rho_{n,p}$  chosen as below.

(i) Under Condition 1 (a), we set  $\tau = (4\gamma + 2)/(4\gamma + 3)$  and  $\rho_{n,p} = \log^{2\gamma+3/2}(p \vee n)$ .

(ii) Under Condition 1 (b), we set  $\tau = 0$  and  $\rho_{n,p} = \sqrt{\log(p \vee n)}$ .

Under Condition 1,  $\{(\mathbf{x}_t, \varepsilon_t)\}_{t=1}^n$  is a linear process with algebraically decaying serial dependence according to the functional dependence measure of Zhang and Wu (2017). Further, (a) permits heavier tail behaviour than that allowed under sub-Gaussianity or sub-exponential distributions when  $\gamma > 1/2$  and  $\gamma > 1$ , respectively. We emphasise that Condition 1 is intended to provide sufficient conditions for Assumptions 2 and 3 to hold. Alternatively, we may directly impose conditions on the data generating process:

**Remark 1.** Medeiros and Mendes (2016), Han and Tsay (2020), Wong et al. (2020) and Adamek et al. (2020) study estimation and inference problems using the Lasso-type estimator (when  $q = 0$ ) while permitting serial dependence by imposing conditions on the mixing coefficients (Davidson, 1994) or functional dependence measures (Wu, 2005, 2011). In the change point literature, Wang and Zhao (2022) propose a change point test and investigate its properties under  $\beta$ -mixing. Xu et al. (2022) analyse the dynamic programming algorithm proposed by Rinaldo et al. (2021) when the functional dependence of  $\{\mathbf{x}_t\}_{t=1}^n$  and  $\{\varepsilon_t\}_{t=1}^n$  decays exponentially. In all above, the tail behaviour of the data is characterised by the sub-Weibull-type decay. This is closely related to, but distinguished from Condition 1 (a) as the latter directly imposes the moment condition on the innovations  $\xi_{it}$ , rather than on  $\mathbf{a}^\top \mathbf{x}_t$  uniformly over all unit vectors  $\mathbf{a} \in \mathbb{R}^p$ .

Corollary 3 follows immediately from Theorem 1 and Proposition 2.

**Corollary 3.** Suppose that Assumptions 1, 4 and 5 and Condition 1 hold, and  $\lambda, r, \eta$  and  $D$  are chosen as in Theorem 1. Then, there exist constants  $c_i > 0, i = 0, 1, 2$ , such that  $\hat{\Theta} = \{\hat{\theta}_j, 1 \leq j \leq \hat{q}: \hat{\theta}_1 < \dots < \hat{\theta}_{\hat{q}}\}$  returned by MOSEG satisfies the following.

(i) Under Condition 1 (a), we have

$$\mathbf{P}\left(\hat{q} = q \text{ and } \max_{1 \leq j \leq q} \delta_j^2 |\hat{\theta}_j - \theta_j| \leq c_0 (\mathfrak{s} \log(p \vee n))^{4\gamma+3}\right) \geq 1 - c_1(p \vee n)^{-c_2}.$$

(ii) Under Condition 1 (b), we have

$$\mathbb{P} \left( \widehat{q} = q \text{ and } \max_{1 \leq j \leq q} \delta_j^2 |\widehat{\theta}_j - \theta_j| \leq c_0 \mathfrak{s} \log(p \vee n) \right) \geq 1 - c_1 (p \vee n)^{-c_2}.$$

In the presence of serial dependence and sub-Weibull tails (through having  $\gamma > 1$  as in Condition 1 (a)), Xu et al. (2022) require that  $\Delta^{(1)} \gtrsim (\mathfrak{s} \log(np))^{4\gamma+2\gamma'-1}$  for the detection of all change points (see (10) for the definition of  $\Delta^{(1)}$ ), where a smaller value of  $\gamma' \in (0, \infty)$  imposes a faster decay of the serial dependence. This is comparable to the condition  $\Delta^{(1)} \gtrsim (\mathfrak{s} \log(np))^{4\gamma+3}$  which is implied by Assumption 5 (a) under Condition 1 (a). We remark that Condition 1 assumes algebraically decaying serial dependence whereas  $\gamma'$  of Xu et al. (2022) governs the rate of exponentially decaying serial dependence.

Corollary 3 (ii) shows that under Gaussianity, the rate of localisation attained by MOSEG matches the minimax lower bound up to  $\log(p \vee n)$ , see Lemma 4 of Rinaldo et al. (2021). At the same time, Assumption 5 (b) translates to  $\Delta^{(1)} \gtrsim \mathfrak{s} \log(p \vee n)$  in this setting, nearly matching the minimax lower bound on the separation rate derived in Lemma 3 of Rinaldo et al. (2021) up to the logarithmic term.

### 3 Multiscale methodology

The single-bandwidth methodology proposed in Section 2 enjoys theoretical consistency as well as computational efficiency, but faces the difficulty arising from identifying a bandwidth that satisfies Assumption 5 (a)–(b) simultaneously. In this section, we propose MOSEG.MS, a multiscale extension of MOSEG, which is shown to achieve theoretical consistency in a parameter space broader than that allowed by Assumption 5, and thus alleviates the difficulty associated with the choice of a single bandwidth.

#### 3.1 MOSEG.MS: Multiscale extension of MOSEG

Similarly to MOSEG, MOSEG.MS consists of moving window-based data scanning and location refinement but it takes a set of bandwidths as an input. The key innovation lies in that for each change point, MOSEG.MS learns the bandwidth best-suited for its detection and localisation from the given set of bandwidths. While there exist methods for multiscale extension of moving window-based change point procedures, mostly developed for univariate time series segmentation (Messer et al., 2014; Cho and Kirch, 2021b), to the best of our knowledge, this is a first attempt at such an extension in a high-dimensional setting. Below we describe MOSEG.MS step-by-step.

**Step 1: Pre-estimator generation.** Given a set of bandwidths  $\mathcal{G} = \{G_h, 1 \leq h \leq H : G_1 < \dots < G_H\}$ , we generate the coarse grid associated with each  $G_h$  and the parameter

$r$  by  $\mathcal{T}_h = \mathcal{T}(r, G_h)$ , see (5). MOSEG.MS produces the sets of pre-estimators  $\tilde{\Theta}(G_h)$  for  $h = 1, \dots, H$ , as in Stage 1 of MOSEG and we denote by  $\tilde{\Theta}(\mathcal{G}) = \cup_{h=1}^H \tilde{\Theta}(G_h)$  the pooled set of all such pre-estimators. Then at each  $\tilde{\theta} \in \tilde{\Theta}(G_h)$ , we have  $T_{\tilde{\theta}}(G_h) > D$  and  $\tilde{\theta} = \arg \max_{k \in \mathcal{I}_{\eta}(\tilde{\theta}) \cap \mathcal{T}_h} T_k(G_h)$ , where  $\mathcal{I}_{\eta}(\tilde{\theta}) = \{\tilde{\theta} - \lfloor \eta G_h \rfloor + 1, \dots, \tilde{\theta} + \lfloor \eta G_h \rfloor\}$  denotes the detection interval associated with  $\tilde{\theta}$ . For simplicity, we write  $\mathcal{I}_1(\tilde{\theta}) = \mathcal{I}(\tilde{\theta})$ . We sometimes write  $\tilde{\theta}(G) \in \tilde{\Theta}(G)$  to make explicit that the pre-estimator is obtained with the bandwidth  $G$ , and denote by  $G(\tilde{\theta})$  the bandwidth involved in the detection of a pre-estimator  $\tilde{\theta}$ . If some  $\tilde{\theta}$  is detected at multiple scales, we treat them distinctly as they are associated with different bandwidths.

**Step 2: Anchor estimator identification.** Next, we identify *anchor* change point estimators  $\tilde{\theta}^A(G) \in \tilde{\Theta}(\mathcal{G})$  which satisfy

$$\bigcup_{h: G_h < G} \bigcup_{k \in \tilde{\Theta}(G_h)} \left\{ \mathcal{I}(k) \cap \mathcal{I}(\tilde{\theta}^A(G)) \right\} = \emptyset. \quad (14)$$

That is, each anchor change point estimator does not have its detection interval overlap with the detection interval of any pre-estimator that is detected with a finer bandwidth. Denote the set of all such anchor change point estimators by  $\tilde{\Theta}^A = \{\tilde{\theta}_j^A, 1 \leq j \leq \hat{q} : \tilde{\theta}_1^A < \dots < \tilde{\theta}_{\hat{q}}^A\}$ , with  $\hat{q} = |\tilde{\Theta}^A|$  as an estimator of the number of change points  $q$ .

**Step 3: Pre-estimator clustering.** We partition (a subset of) the pre-estimators in  $\tilde{\Theta}(\mathcal{G})$  into  $\mathcal{C}_j$ ,  $j = 1, \dots, \hat{q}$  as described below. Initialised as  $\mathcal{C}_j = \emptyset$ , for each  $j$ , we add to  $\mathcal{C}_j$  the  $j$ th anchor estimator  $\tilde{\theta}_j^A$  as well as all  $\tilde{\theta} \in \tilde{\Theta}(\mathcal{G})$  which simultaneously fulfil

$$\begin{aligned} \mathcal{I}(\tilde{\theta}) \cap \mathcal{I}(\tilde{\theta}_j^A) &\neq \emptyset, \quad \text{and} \\ \{\tilde{\theta} - G(\tilde{\theta}) - \lfloor G(\tilde{\theta})/2 \rfloor + 1, \dots, \tilde{\theta} + G(\tilde{\theta}) + \lfloor G(\tilde{\theta})/2 \rfloor\} \cap \mathcal{I}(\tilde{\theta}_{j'}^A) &= \emptyset \text{ for all } j' \neq j. \end{aligned} \quad (15)$$

**Step 4: Location refinement.** For a given cluster  $\mathcal{C}_j$ , we denote the smallest and the largest bandwidths associated with the detection of the pre-estimators in  $\mathcal{C}_j$ , by  $G_j^m$  and  $G_j^M$ , respectively, and the corresponding pre-estimators by  $\tilde{\theta}_j^m$  and  $\tilde{\theta}_j^M$  (when  $|\mathcal{C}_j| = 1$ , we have  $\tilde{\theta}_j^m = \tilde{\theta}_j^M$  and  $G_j^m = G_j^M$ ). Setting  $G_j^* = \lfloor 3G_j^m/4 + G_j^M/4 \rfloor$ , we identify the local minimiser of the objective function defined in (7) for all  $j = 1, \dots, \hat{q}$ , as

$$\begin{aligned} \check{\theta}_j &= \arg \min_{\tilde{\theta}_j^m - G_j^* + 1 \leq k \leq \tilde{\theta}_j^m + G_j^*} Q\left(k; \tilde{\theta}_j^m - G_j^*, \tilde{\theta}_j^m + G_j^*, \hat{\beta}_j^L, \hat{\beta}_j^R\right), \\ \text{with } \hat{\beta}_j^L &= \hat{\beta}_{(\tilde{\theta}_j^m - G_j^*) \vee 0, \tilde{\theta}_j^m - G_j^*} \quad \text{and} \quad \hat{\beta}_j^R = \hat{\beta}_{\tilde{\theta}_j^m + G_j^m, (\tilde{\theta}_j^m + G_j^m + G_j^*) \wedge n}. \end{aligned} \quad (16)$$

The set of final estimators is denoted by  $\check{\Theta} = \{\check{\theta}_j, 1 \leq j \leq \hat{q}\}$ .

An algorithmic description of MOSEG.MS is given in Algorithm 2 of Appendix D. The identification of anchor change point estimators bears some resemblance with the bottom-up merging

proposed in Messer et al. (2014), but the anchor estimators do not come with a guaranteed rate of localisation. Instead, we cluster the pre-estimators and learn the bandwidth  $G_j^*$  well-suited for localising each  $\theta_j$  in a data-driven way, with which we perform the location refinement step.

**Remark 2** (Bandwidth generation). Cho and Kirch (2021b) propose to use  $\mathcal{G}$  generated as a sequence of Fibonacci numbers, for a multiscale extension of the moving sum procedure proposed in Eichinger and Kirch (2018) in the context of univariate mean change point detection. Given  $G_0 = G_1$ , we iteratively produce  $G_h$ ,  $h \geq 2$ , as  $G_h = G_{h-1} + G_{h-2}$ . Equivalently, we set  $G_h = F_h G_0$  where  $F_h = F_{h-1} + F_{h-2}$  with  $F_0 = F_1 = 1$ . This is repeated until for some  $H$ , it holds that  $G_H < \lfloor n/2 \rfloor$  while  $G_{H+1} \geq \lfloor n/2 \rfloor$ . By induction, it is easily seen that  $F_h = O((1 + \sqrt{2})/2)^h$  such that the thus-generated bandwidth set  $\mathcal{G}$  satisfies  $|\mathcal{G}| = O(\log(n))$ .

**Remark 3** (Computational complexity). Let  $\text{Lasso}(a, b)$  denote the cost of solving a Lasso problem with sample size  $a$  and dimensionality  $b$ , and recall that the parameter  $r$  determines the coarseness of the grid  $\mathcal{T}$  in Stage 1 of MOSEG. Then, the computational costs of Stages 1 and 2 of MOSEG are  $O(n/(rG) \cdot \text{Lasso}(G, p))$  and  $O(2q \cdot \text{Lasso}(G, p) + np)$ , respectively, where the first stage dominates the overall complexity. Similarly, with the set of bandwidths generated as described in Remark 2, the complexity of the multiscale extension MOSEG.MS is dominated by Step 1 for pre-estimator generation, which amounts to  $O(n/(rG_1) \cdot \text{Lasso}(n, p))$  with  $G_1$  denoting the finest scale. This follows from that  $\sum_{h=1}^H n/(rG_h) \leq n/(rG_1) \sum_{h=1}^{\infty} F_h^{-1} = O(n/(rG_1))$ .

### 3.2 Consistency of MOSEG.MS

We make the following assumption on the size of change  $\delta_j$  and the spacing between the neighbouring change points.

**Assumption 5'**. Let  $\mathcal{G}$  denote the set of bandwidths generated as in Remark 2 with  $G_1 \geq C_0 \max\{\rho_{n,p}^2, (\omega^{-1} \mathfrak{s} \log(p))^{1/(1-\tau)}\}$ . Then, for each change point  $\theta_j$ ,  $j = 1, \dots, q$ , there exists a bandwidth  $G_{(j)} \in \mathcal{G}$  such that

- (a)  $4G_{(j)} \leq \min(\theta_{j+1} - \theta_j, \theta_j - \theta_{j-1})$ , and
- (b)  $\delta_j^2 G_{(j)} \geq 4C_1 \max\left\{\omega^{-2} \mathfrak{s} \rho_{n,p}^2, (\omega^{-1} \mathfrak{s} \log(p))^{1/(1-\tau)}\right\}$  with  $C_1$  from Assumption 5.

If there are multiple such bandwidths, let  $G_{(j)}$  denote the smallest one.

Assumption 5' relaxes Assumption 5 by requiring that for each  $\theta_j$ , there exists one bandwidth  $G_{(j)} \in \mathcal{G}$  fulfilling the requirements imposed on a single bandwidth in the latter for all  $j = 1, \dots, q$ . Assumption 5' effectively places a condition on

$$\Delta^{(2)} = \min_{1 \leq j \leq q} \delta_j^2 \cdot \min(\theta_{j+1} - \theta_j, \theta_j - \theta_{j-1}) \quad (17)$$

for MOSEG.MS to detect all  $q$  changes. Compared to  $\Delta^{(1)}$  defined in (10), we always have  $\Delta^{(1)} \leq \Delta^{(2)}$  and, if frequent large changes and small changes over long stretches of stationarity are simultaneously present, the former can be considerably smaller than the latter, see also the discussion in Cho and Kirch (2021a). To the best of our knowledge, Theorem 4 below provides a first result obtained under the larger parameter space defined with  $\Delta^{(2)}$ , in establishing the consistency of a data segmentation methodology for the problem in (1). We refer to Appendix A for further discussions and comprehensive comparison between MOSEG, MOSEG.MS and competing methodologies.

**Theorem 4.** Suppose that Assumptions 1, 2, 3, 4 and 5' hold. Let the tuning parameters satisfy  $\lambda \geq 4C_{\text{DEV}}\rho_{n,p}$ ,  $r \in [G_1^{-1}, 1/4)$ ,  $\eta \in (4r, 1]$  and

$$\frac{48\sqrt{\mathfrak{s}}\lambda}{\omega} < D < \frac{\eta}{4\sqrt{2}} \min_{1 \leq j \leq q} \delta_j \sqrt{G_{(j)}}. \quad (18)$$

Then, there exists a constant  $c_0 > 0$  such that on  $\mathcal{D}^{(1)} \cap \mathcal{D}^{(2)} \cap \mathcal{R}^{(1)} \cap \mathcal{R}^{(2)}$ , MOSEG.MS returns  $\check{\Theta} = \{\check{\theta}_j, 1 \leq j \leq \hat{q}: \check{\theta}_1 < \dots < \check{\theta}_{\hat{q}}\}$  which satisfies

$$\hat{q} = q \quad \text{and} \quad \max_{1 \leq j \leq q} \delta_j^2 |\check{\theta}_j - \theta_j| \leq c_0 \max \left( \mathfrak{s} \rho_{n,p}^2, (\mathfrak{s} \log(p))^{-\frac{1}{1-\tau}} \right).$$

**Corollary 5.** Suppose that Assumptions 1, 4 and 5' and Condition 1 hold, and  $\lambda$ ,  $r$  and  $D$  are chosen as in Theorem 4. Then, there exist constants  $c_i > 0$ ,  $i = 0, 1, 2$ , such that  $\check{\Theta} = \{\check{\theta}_j, 1 \leq j \leq \hat{q}: \check{\theta}_1 < \dots < \check{\theta}_{\hat{q}}\}$  returned by MOSEG.MS satisfies the following.

(i) Under Condition 1 (a), we have

$$\mathbb{P} \left( \hat{q} = q \quad \text{and} \quad \max_{1 \leq j \leq q} \delta_j^2 |\check{\theta}_j - \theta_j| \leq c_0 (\mathfrak{s} \log(p \vee n))^{4+3\gamma} \right) \geq 1 - c_1 (p \vee n)^{-c_2}.$$

(ii) Under Condition 1 (b), we have

$$\mathbb{P} \left( \hat{q} = q \quad \text{and} \quad \max_{1 \leq j \leq q} \delta_j^2 |\check{\theta}_j - \theta_j| \leq c_0 \mathfrak{s} \log(p \vee n) \right) \geq 1 - c_1 (p \vee n)^{-c_2}.$$

## 4 Simulation studies

### 4.1 Choice of tuning parameters

We discuss the selection of tuning parameters required for the application of MOSEG.MS, namely the set of bandwidths  $\mathcal{G}$ , the grid  $\mathcal{T}(r, G)$  in (5),  $\eta \in (0, 1]$  involved in the pre-estimation of the change points (see (6)), the penalty parameter  $\lambda$  and the threshold  $D$ .

**Selection of  $\mathcal{G}$ .** In selecting  $\mathcal{G}$ , we need to ensure that the parameter estimators obtained with the finest bandwidth  $G_1$  are good enough for the purpose of change point detection even for high dimensions. To gain insights about the minimum sample size requirement with respect to  $p$  and  $\mathfrak{s}$ , we performed numerical experiments by simulating datasets under (1) with  $q = 0$  and varying  $(n, p, \mathfrak{s}, G)$ , and recording the relative  $\ell_2$ -error  $\max_{0 \leq k \leq n-G} |\beta_0|_2^{-1} |\hat{\beta}_{k,k+G} - \beta_0|_2$  for each realisation. Then, regressing the 90%-percentile of the estimation errors over 100 realisations onto  $\log(G)$ ,  $\log \log(p)$  and  $\log \log(n)$  ( $R^2 = 0.8945$ ), we obtain a simple rule to determine the finest bandwidth as  $G_1 = G_1(n, p) = \exp(c_0 - c_1 \log \log(n) + c_2 \log \log(p))$  with pre-specified  $c_i > 0$ ,  $i = 0, 1, 2$ . Adopting the Fibonacci rule in Remark 2 often gives a sequence of bandwidths that grows too quickly when the sample size  $n$  is small. Therefore, with the finest bandwidth  $G_1$  chosen as above, we recommend generating bandwidths as  $G_h = (h + 2)/3 \cdot G_1$  for  $h \geq 2$ . Throughout the simulation studies and real data applications, we set  $H = 3$ .

**Selection of  $D$  and  $\lambda$ .** As seen in Theorems 1 and 4, the theoretically valid choices of  $\lambda$  and  $D$  involve typically unknown parameters. For their simultaneous selection, we adopt a cross validation (CV) method motivated by Zou et al. (2020). We set the odd-indexed observations  $(Y_t, \mathbf{x}_t)$ ,  $t \in \mathcal{J}_1 = \{2t + 1, t = 0, \dots, \lfloor (n - 1)/2 \rfloor\}$  for model training, and the even-indexed observations  $(Y_t, \mathbf{x}_t)$ ,  $t \in \mathcal{J}_0 = \{1, \dots, n\} \setminus \mathcal{J}_1$  for model validation. Let  $\Lambda$  denote the grid of possible values for  $\lambda$ . For given  $G \in \mathcal{G}$  and  $\lambda \in \Lambda$ , we generate  $\tilde{\Theta}(G, \lambda) = \{\tilde{\theta}_j(G, \lambda), 1 \leq j \leq \tilde{q}_0(G, \lambda)\}$ , the set of pre-estimators obtained from the whole sample with  $D = 0$ , i.e. we take all local maximisers of the MOSUM statistics according to (6); due to the detection rule, we always have  $\tilde{q}_0(G, \lambda) \leq n/(2\eta G)$ . Sorting the elements of  $\tilde{\Theta}(G, \lambda)$  in the decreasing order of the associated MOSUM detector values, we generate a sequence of nested change point models

$$\emptyset = \tilde{\Theta}_{[0]}(G, \lambda) \subset \tilde{\Theta}_{[1]}(G, \lambda) \subset \dots \subset \tilde{\Theta}_{[\tilde{q}_0(G, \lambda)]}(G, \lambda) = \tilde{\Theta}(G, \lambda).$$

Then, we evaluate the CV score on the validation set, as

$$\begin{aligned} \text{CV}(G, \lambda, m) &= \text{RSS}_0(\tilde{\Theta}_{[m]}(G, \lambda), \lambda), \quad \text{where} \\ \text{RSS}_0(\mathcal{L}, \lambda) &= \sum_{j=0}^L \sum_{\substack{t \in \mathcal{J}_0 \cap \\ \{\ell_j+1, \dots, \ell_{j+1}\}}} \left( Y_t - \mathbf{x}_t^\top \hat{\beta}_j^{(1)}(\lambda) \right)^2 \end{aligned}$$

for any  $\mathcal{L} = \{\ell_j, 1 \leq \ell_j \leq L : 0 = \ell_0 < \ell_1 < \dots < \ell_L < \ell_{L+1} = n\}$ . Here,  $\hat{\beta}_j^{(1)}(\lambda)$  denotes the Lasso estimator obtained using  $(Y_t, \mathbf{x}_t)$ ,  $t \in \mathcal{J}_1 \cap \{\ell_j, \dots, \ell_{j+1}\}$  with the penalty parameter  $\lambda$ . Then for each  $G_h \in \mathcal{G}$ , we find

$$(\lambda^*, m^*) = \arg \min_{\substack{(\lambda, m): \lambda \in \Lambda, \\ 0 \leq m \leq \tilde{q}_0(G_h, \lambda)}} \text{CV}(G_h, \lambda, m)$$

and obtain the set of pre-estimators  $\tilde{\Theta}(G_h)$  using  $\lambda^*$  and  $m^*$ , attaining the local maximisers associated with the  $m^*$  largest MOSUM detector values. Note that this amounts to selecting the bandwidth-dependent threshold  $D$  at a value just below the  $m^*$ th largest MOSUM detector value. Such  $\tilde{\Theta}(G_h)$ ,  $G_h \in \mathcal{G}$ , serve as an input to Steps 2–4 of MOSEG.MS.

**Selection of other tuning parameters.** We do not find the performance of MOSEG and MOSEG.MS sensitive to the choice of  $\eta$ , and recommend  $\eta = 0.75$  based on extensive simulations. As noted in Remark 3 and also in Appendix A, MOSEG.MS is highly competitive computationally against the existing methods, and this is further verified in the runtime exercise presented in Section 4.4 below. Therefore, we report the results obtained with  $r = G^{-1}$  (the most dense grid) in the main text and provide the results obtained with  $r = 1/10$  in Appendix B.1.

## 4.2 Simulation settings

We apply MOSEG.MS to datasets simulated with varying  $(n, p, \mathfrak{s})$  and change point configurations. In each setting, we generate  $\mathbf{x}_t$  as i.i.d. Gaussian random vectors with mean  $\mathbf{0}$  and the covariance matrix  $\Sigma_x$  which are specified below, and  $\varepsilon_t \sim_{\text{iid}} \mathcal{N}(0, \sigma_\varepsilon^2)$ ; unless specified otherwise, we use  $\sigma_\varepsilon = 1$ . We report the results from non-Gaussian and serially dependent data in Appendix B.2 where overall, the results are not sensitive to tail behaviour or temporal dependence. In what follows, we assume that for given  $(p, \mathfrak{s})$  and  $\mathcal{S} \subset \{1, \dots, p\}$  with  $|\mathcal{S}| = \mathfrak{s}$ , the parameter vector  $\beta_0 = (\beta_{0,1}, \dots, \beta_{0,p})^\top \in \mathbb{R}^p$  has  $\beta_{0,i} \neq 0$  for  $i \in \mathcal{S}$  and  $\beta_{0,i} = 0$  otherwise, i.e.  $\mathcal{S}$  is the support of  $\beta_0$ . For each setting, we generate 100 realisations.

- (M1) Setting  $p = 100$ ,  $q = 3$  and  $\Sigma_x = \mathbf{I}$ , we vary  $n \in \{480, 560, 640, 720, 800\}$  and the change points are located at  $\theta_j = jn/4$ ,  $j = 1, 2, 3$ . Fixing  $\mathcal{S} = \{1, \dots, \mathfrak{s}\}$  with  $\mathfrak{s} = 4$ , we set  $\beta_{0,i} = 0.4 \cdot (-1)^{i-1}$  for  $i \in \mathcal{S}$  and  $\beta_j = (-1)^j \cdot \beta_0$ .
- (M2) We set  $n = 300$ ,  $p = 100$  and  $q = 2$ , and  $\Sigma_x = [0.6^{|i-i'|}]_{i,i'=1}^p$ . The change points are located at  $\theta_j = jn/3$ ,  $j = 1, 2$ , and we vary  $\mathfrak{s} \in \{10, 20, 30\}$ . For each realisation, we randomly draw  $\mathcal{S} \subset \{1, \dots, p\}$  of size  $\mathfrak{s}$ , and set  $\beta_{0,i} = 1/\sqrt{4\mathfrak{s}}$  for  $i \in \mathcal{S}$ ,  $\beta_j = (-1)^j \cdot \beta_0$ .
- (M3) We have  $n = 300$ ,  $p = 100$ ,  $q = 2$ ,  $\mathfrak{s} = 10$  and  $\Sigma_x = [0.6^{|i-i'|}]_{i,i'=1}^p$ . The change points are located at  $\theta_j = jn/3$  and fixing  $\mathcal{S} = \{1, \dots, \mathfrak{s}\}$ , we set  $\beta_{0,i} = \delta \cdot (-1)^{i-1}$  for  $i \in \mathcal{S}$  with varying  $\delta \in \{0.2, 0.4, 0.8, 1.6\}/\sqrt{\mathfrak{s}}$ , and  $\beta_j = (-1)^j \cdot \beta_0$ .
- (M4) We set  $n = 840$ ,  $p = 50$ ,  $q = 5$ ,  $\mathfrak{s} = 10$  and  $\Sigma_x = \mathbf{I}$ . The change points are located at  $\theta_1 = 60$ ,  $\theta_2 = 120$ ,  $\theta_3 = 240$ ,  $\theta_4 = 360$  and  $\theta_5 = 600$  and fixing  $\mathcal{S} = \{1, \dots, \mathfrak{s}\}$ , we set  $\beta_{0,i} = \delta \cdot (-1)^{i-1}$  for  $i \in \mathcal{S}$  with varying  $\delta \in \{0.2, 0.4, 0.8, 1.6\}/\sqrt{\mathfrak{s}}$ , and  $\beta_1 = -\beta_2 = -2\beta_0$ ,  $\beta_3 = -\beta_4 = -\sqrt{2}\beta_0$  and  $\beta_5 = -\beta_6 = -\beta_0$ .

(M5) The data is generated as in (M3) except for that  $q = 0$ ,  $\Sigma_x = [10^2 \cdot 0.6^{|i-i'|}]_{i,i'=1}^p$  and  $\sigma_\varepsilon = 10$ , and we use  $\delta \in \{1, 1.2, 1.4, 1.6\}$ .

In settings (M1)–(M3), we vary  $n$ ,  $\mathfrak{s}$  and  $\delta$  determining the size of changes. In setting (M4), the change points are multiscale in the sense that the size of change and spacing between the change points vary, but  $\delta_j^2 \cdot \min(\theta_{j+1} - \theta_j, \theta_j - \theta_{j-1})$  is kept constant for  $j = 1, 3, 5$  and  $j = 2, 4$ , respectively. This results in  $\Delta^{(1)}$  in (10) being much smaller than  $\Delta^{(2)}$  in (17). (M5) is designed to test the performance of data segmentation methods when  $q = 0$ , where we scale the data to examine the sensitivity of the tuning parameter choices discussed in Section 4.1.

### 4.3 Simulation results

We apply MOSEG.MS with the tuning parameters selected as described in Section 4.1. For the purpose of illustration only, we also apply MOSEG with the bandwidth set ‘optimally’ in terms of its detection power; for (M1)–(M3) where change points are evenly spaced, we set  $G = 3/4 \cdot \min_{0 \leq j \leq q} (\theta_{j+1} - \theta_j)$ . For (M4) with multiscale change points, there does not exist a single bandwidth that works well in detecting all change points so we simply set  $G = 125$ . For (M5) with  $q = 0$ , we set  $G = G_1$  selected as described in Section 4.1. For comparison, we apply the VPWBS method proposed by Wang et al. (2021) with the default tuning parameters recommended by the authors. We also considered the methods proposed by Kaul et al. (2019a) and Rinaldo et al. (2021) but generally they performed poorly for the simulation models considered in this paper and we omit the results from these methods.

In Tables 1–4, we report the distribution of the bias in change point number estimation ( $\hat{q} - q$ ) for each method over the 100 realisations generated under each setting. Additionally, we report the average of the scaled Hausdorff distance between the sets of estimated and true change points, denoted by  $\hat{\Theta}$  and  $\Theta$  respectively,

$$d_H(\hat{\Theta}, \Theta) = \frac{1}{n} \max \left\{ \max_{\hat{\theta} \in \hat{\Theta}} \min_{\theta \in \Theta} |\hat{\theta} - \theta|, \max_{\theta \in \Theta} \min_{\hat{\theta} \in \hat{\Theta}} |\hat{\theta} - \theta| \right\}, \quad (19)$$

over 100 realisations. Here, we use the convention that  $\mathcal{D}(\emptyset, \Theta) = 1$ . In Table 5, we report the proportion of detected false positives when  $q = 0$ .

Generally, as expected, we observe better performance from all methods with increasing spacing between the change points in (M1) or increasing  $\delta$  in (M3)–(M4) while varying  $\mathfrak{s}$  brings in less clear change in the performance. In the presence of homogeneous change points under (M1)–(M3), MOSEG performs well in terms of correctly estimating the number of change points, but it suffers from its lack of adaptivity in the presence of multiscale change points under (M4). Overall, between MOSEG and MOSEG.MS, we observe better localisation performance from the latter, but this is possibly because the Hausdorff distance tends to favour the cases when the change points are over-detected. With the use of multiple bandwidths, MOSEG.MS sometimes over-estimates the number of change points compared to MOSEG.



Comparing the performance of MOSEG.MS and VPWBS, we note that the former generally attains better detection power. VPWBS performs marginally better than MOSEG.MS when  $\Sigma_x = \mathbf{I}$  as in (M1), but it behaves worse when  $\Sigma_x$  deviates from the identity matrix in (M2) and (M3), possibly since VPWBS relies on identifying a good projection direction that is influenced by the cross-sectional dependence. Under (M5), where no changes are present, our methods are shown to control the number of false positives well. Here, we do not include VPWBS as it tends to detect false positives in most cases, which may be attributed to the lack of scale adaptivity in the tuning parameters chosen by default.

Table 1: (M1) Performance of MOSEG, MOSEG.MS and VPWBS over 100 realisations.

$n$	Method	$\hat{q} - q$							$d_H$
		-3	-2	-1	0	1	2	$\geq 3$	
480	MOSEG	2	3	8	87	0	0	0	0.1079
	MOSEG.MS	2	1	6	90	1	0	0	0.0593
	VPWBS	1	3	14	58	16	5	3	0.0795
560	MOSEG	0	0	1	99	0	0	0	0.0310
	MOSEG.MS	0	0	6	89	5	0	0	0.0284
	VPWBS	1	0	10	73	5	8	3	0.0579
640	MOSEG	1	0	2	97	0	0	0	0.0421
	MOSEG.MS	0	0	7	91	2	0	0	0.0253
	VPWBS	0	1	3	89	3	2	2	0.0291
720	MOSEG	0	0	0	100	0	0	0	0.0235
	MOSEG.MS	0	0	2	85	13	0	0	0.0239
	VPWBS	0	0	1	92	3	3	1	0.0190
800	MOSEG	0	0	0	100	0	0	0	0.0186
	MOSEG.MS	0	0	0	83	14	3	0	0.0129
	VPWBS	0	0	2	92	3	2	1	0.0202

Table 2: (M2) Performance of MOSEG, MOSEG.MS and VPWBS over 100 realisations.

$s$	Method	$\hat{q} - q$						$d_H$
		-2	-1	0	1	2	$\geq 3$	
10	MOSEG	20	35	45	0	0	0	0.3288
	MOSEG.MS	14	46	36	4	0	0	0.3331
	VPWBS	45	17	11	9	15	3	0.2465
20	MOSEG	24	28	48	0	0	0	0.3425
	MOSEG.MS	10	47	42	1	0	0	0.2869
	VPWBS	44	13	18	13	9	3	0.2302
30	MOSEG	22	27	51	0	0	0	0.3250
	MOSEG.MS	13	27	56	4	0	0	0.2587
	VPWBS	24	20	33	9	9	5	0.1843

Table 3: (M3) Performance of MOSEG, MOSEG.MS and VPWBS over 100 realisations.

$\sqrt{10}\delta$	Method	$\hat{q} - q$						$d_H$
		-2	-1	0	1	2	$\geq 3$	
0.2	MOSEG	24	35	35	6	0	0	0.4110
	MOSEG.MS	11	47	39	3	0	0	0.3219
	VPWBS	77	9	5	6	1	2	0.3025
0.4	MOSEG	24	26	44	6	0	0	0.3816
	MOSEG.MS	12	40	45	3	0	0	0.3204
	VPWBS	53	20	12	8	4	3	0.2681
0.8	MOSEG	8	13	77	2	0	0	0.1618
	MOSEG.MS	2	28	69	1	0	0	0.1468
	VPWBS	13	7	58	14	6	2	0.1061
1.6	MOSEG	0	2	97	1	0	0	0.0274
	MOSEG.MS	1	5	94	0	0	0	0.0420
	VPWBS	1	1	84	10	4	0	0.0404

Table 4: (M4) Performance of MOSEG, MOSEG.MS and VPWBS over 100 realisations.

$\sqrt{10}\delta$	Method	$\hat{q} - q$							$d_H$
		-3	-2	-1	0	1	2	$\geq 3$	
0.2	MOSEG	92	5	3	0	0	0	0	0.8577
	MOSEG.MS	19	20	18	16	20	5	2	0.2366
	VPWBS	95	1	2	1	1	0	0	0.4073
0.4	MOSEG	95	2	2	1	0	0	0	0.8969
	MOSEG.MS	16	18	23	22	14	7	0	0.2120
	VPWBS	73	2	7	6	7	5	0	0.3247
0.8	MOSEG	72	2	26	0	0	0	0	0.7650
	MOSEG.MS	3	9	43	28	13	3	1	0.1213
	VPWBS	13	40	29	11	4	2	1	0.1165
1.6	MOSEG	61	0	38	1	0	0	0	0.6953
	MOSEG.MS	0	0	91	8	1	0	0	0.0619
	VPWBS	3	35	38	19	1	3	1	0.0900

#### 4.4 Comparison of runtime

In this section, we investigate the runtime of the proposed methodology.<sup>1</sup> We generate the data as described in (M3) with  $\delta = 1.6$  while varying  $n$  and  $p$ . Specifically, in the left panel of Figure 1, we fix  $n = 450$  while varying  $p \in \{80, 100, 120, \dots, 220\}$  and in the right panel, we fix  $p = 100$  while varying  $n \in \{240, 300, 360, \dots, 660\}$ .

We report the runtime of MOSEG.MS applied with  $\mathcal{G}$  chosen as recommended, the finest grid (i.e.  $\mathcal{T} = \{G, \dots, n - G\}$ ) and the CV-based model selection described in Section 4.1, and MOSEG applied with  $G = n/6$ . For comparison, we consider VPWBS (Wang et al., 2021), DP (Rinaldo et al., 2021) and ARBSEG (Kaul et al., 2019a) applied with the recommended tuning parameters. Both MOSEG and MOSEG.MS take only a fraction of time taken by

<sup>1</sup>This work was carried out using the computational facilities of the Advanced Computing Research Centre at the University of Bristol. Three points were used from a single Lenovo nx360 m5 node with two 14 core 2.4 GHz Intel E5-2680 v4 (Broadwell) CPUs.

Table 5: (M5) Proportions of detecting false positives when  $q = 0$  for MOSEG and MOSEG.MS over 100 realisations.

Method	$\delta$			
	1	1.2	1.4	1.6
MOSEG	0.05	0.01	0.01	0.02
MOSEG.MS	0.04	0.01	0.01	0.02

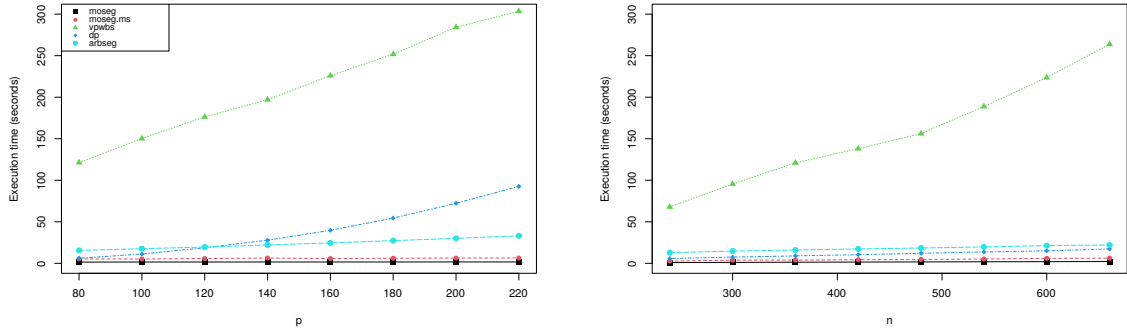


Figure 1: Execution time in seconds of MOSEG, MOSEG.MS, VPWBS, DP and ARBSEG. Left:  $p$  varies while  $n = 450$  is fixed. Right:  $n$  varies while  $p = 100$  is fixed.

the competing methodologies in their computation even without the use of the coarse grid, and their runtime does not vary much with increasing  $n$  or  $p$  in the ranges considered. As expected, MOSEG is faster than MOSEG.MS but the difference in execution time is much smaller than that between MOSEG.MS and other competitors. Out of the five methods considered, VPWBS is the slowest possibly as it requires a large number of group Lasso fits.

## 5 Real data applications

### 5.1 Arctic sea ice extent

Arctic sea ice extent (SIE), defined as the land area covered with at least 15% ice concentration, is a key determinant in the Arctic ecosystem, and it is an indicator of climate change (Serreze and Meier, 2019). We model  $Y_t$ , the first difference of the gridded monthly mean SIE measured between February 1984 and December 2018, with the regressors  $\mathbf{x}_t$  consisting of the measurements of 18 variables taken in the previous three months, see Table E.1 in Appendix E for the list of the 18 variables. In total, we have  $n = 418$  and  $p = 55$  including the intercept. Analysing the same dataset, Coulombe and Göbel (2021) noted possible nonstationarities in the data, which supports the piecewise stationary modelling approach taken here. We account for any seasonality by removing the monthly averages from both SIE and the regressors. We also take the first difference of CO2, one of the 18 variables, to ensure the covariance stationarity of  $\mathbf{x}_t$ , and each covariate series is scaled to have unit standard deviation.

Using MOSEG.MS with bandwidths  $\mathcal{G} = \{60, 80, 100\}$  chosen as recommended in Section 4.1,



intercept.

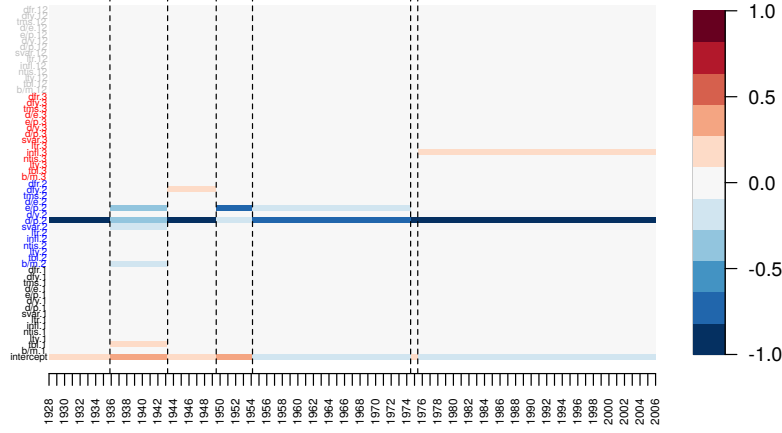


Figure 3: Equity premium data: Parameter estimates from each estimated segment obtained by MOSEG.MS. Variables at different lags are coloured differently in the  $y$ -axis.

We apply MOSEG.MS with  $\mathcal{G} = \{72, 96, 120\}$  in line with the choice described in Section 4.1 but we select  $G_h$  to be multiples of 12 for interpretability as the observation frequency is monthly. MOSEG.MS returns  $\hat{q} = 6$  change point estimators reported in Table 6. In Figure 3, we plot the local parameter estimates obtained from each of the seven estimated segments. We can relate the change detected in 1954 to the findings reported in Rapach et al. (2010), where they attribute the instability in the pairwise relationships between the equity premium and each of the 14 variables to the Treasury-Federal Reserve Accord and the transition from the wartime economy. Dividend price ratio (d/p) is deemed relevant throughout the observation period which is in accordance with the observations made in Welch and Goyal (2008). They also remark that the recession from 1973 to 1975 due to the Oil Shock drives the good predictive performance of many models proposed for equity premium forecasting, and most perform poorly over the 30 year period (1975–2005) following the Oil Shock. The two last segments defined by the change point estimators reported in Table 6 coincide with these important periods, which supports the validity of the segmentation returned by MOSEG.MS. We note that regardless of the choice of bandwidths, both of the two estimators in 1974 and 1975 defining the two periods are detected separately.

Table 6: Equity premium data: Change point estimators detected by MOSEG.MS.

Estimator	$\hat{\theta}_1$	$\hat{\theta}_2$	$\hat{\theta}_3$	$\hat{\theta}_4$	$\hat{\theta}_5$	$\hat{\theta}_6$
Date	Oct 1935	Mar 1943	Jun 1949	Feb 1954	Jun 1974	May 1975

## 6 Conclusions

In this paper, we propose MOSEG, a high-dimensional data segmentation methodology for detecting multiple changes in the parameters under a linear regression model. It proceeds in two steps, first scanning the data for large changes in local parameter estimators over a moving window, followed by a computational efficient location refinement step. We further propose its multiscale extension, MOSEG.MS, which alleviates the necessity to select a single bandwidth. We derive the theoretical consistency of MOSEG and MOSEG.MS in a general setting permitting serial dependence and heavy tails and show their (near-)minimax optimality under Gaussianity. In particular, the consistency of MOSEG.MS is guaranteed in a parameter space simultaneously permitting large changes over short intervals and small changes over long stretches of stationarity, and thus is much broader than that typically adopted in the literature. Comparative simulation studies demonstrate the competitiveness of the proposed methodologies, and findings from the application of MOSEG.MS to real datasets on Arctic sea ice extent and equity premium datasets support its efficacy.

## Acknowledgements

Haeran Cho is supported by the Leverhulme Trust (RPG-2019-390). Dom Owens was supported by a studentship from Compass, the EPSRC Centre for Doctoral Training in Computational Statistics and Data Science.

## References

- Adamek, R., Smeekes, S., and Wilms, I. (2020). Lasso inference for high-dimensional time series. *arXiv preprint arXiv:2007.10952*.
- Bai, J. and Perron, P. (1998). Estimating and testing linear models with multiple structural changes. *Econometrica*, pages 47–78.
- Bai, Y. and Safikhani, A. (2022). A unified framework for change point detection in high-dimensional linear models. *arXiv preprint arXiv:2207.09007*.
- Basu, S. and Michailidis, G. (2015). Regularized estimation in sparse high-dimensional time series models. *The Annals of Statistics*, 43(4):1535–1567.
- Bühlmann, P. and van de Geer, S. (2011). *Statistics for High-dimensional Data: Methods, Theory and Applications*. Springer Science & Business Media.
- Chen, L., Wang, W., and Wu, W. B. (2021). Inference of breakpoints in high-dimensional time series. *Journal of the American Statistical Association*, pages 1–33.
- Cho, H. and Kirch, C. (2021a). Data segmentation algorithms: Univariate mean change and beyond. *Econometrics and Statistics*, To Appear.
- Cho, H. and Kirch, C. (2021b). Two-stage data segmentation permitting multiscale change

- points, heavy tails and dependence. *Annals of the Institute of Statistical Mathematics*, 74(4):1–32.
- Cho, H., Maeng, H., Eckley, I. A., and Fearnhead, P. (2022). High-dimensional time series segmentation via factor-adjusted vector autoregressive modelling. *arXiv preprint arXiv:2204.02724*.
- Coulombe, P. G. and Göbel, M. (2021). Arctic amplification of anthropogenic forcing: a vector autoregressive analysis. *Journal of Climate*, 34(13):5523–5541.
- Datta, A., Zou, H., and Banerjee, S. (2019). Bayesian high-dimensional regression for change point analysis. *Statistics and its Interface*, 12(2):253.
- Davidson, J. (1994). *Stochastic Limit Theory: An Introduction for Econometricians*. OUP Oxford.
- Eichinger, B. and Kirch, C. (2018). A mosum procedure for the estimation of multiple random change points. *Bernoulli*, 24(1):526–564.
- Fryzlewicz, P. (2014). Wild binary segmentation for multiple change-point detection. *The Annals of Statistics*, 42(6):2243–2281.
- Gao, F. and Wang, T. (2022). Sparse change detection in high-dimensional linear regression. *arXiv preprint arXiv:2208.06326*.
- Han, Y. and Tsay, R. S. (2020). High-dimensional linear regression for dependent data with applications to nowcasting. *Statistica Sinica*, 30(4):1797–1827.
- Kaul, A., Jandhyala, V. K., and Fotopoulos, S. B. (2019a). Detection and estimation of parameters in high dimensional multiple change point regression models via  $l_1/l_0$  regularization and discrete optimization. *arXiv preprint arXiv:1906.04396*.
- Kaul, A., Jandhyala, V. K., and Fotopoulos, S. B. (2019b). An efficient two step algorithm for high dimensional change point regression models without grid search. *Journal of Machine Learning Research*, 20(111):1–40.
- Kirch, C. and Reckrühm, K. (2022). Data segmentation for time series based on a general moving sum approach. *arXiv preprint arXiv:2207.07396*.
- Koo, B., Anderson, H. M., Seo, M. H., and Yao, W. (2020). High-dimensional predictive regression in the presence of cointegration. *Journal of Econometrics*, 219(2):456–477.
- Lee, S., Seo, M. H., and Shin, Y. (2016). The lasso for high dimensional regression with a possible change point. *Journal of the Royal Statistical Society: Series B (Statistical Methodology)*, 78(1):193.
- Leonardi, F. and Bühlmann, P. (2016). Computationally efficient change point detection for high-dimensional regression. *arXiv preprint arXiv:1601.03704*.
- Liu, B., Qi, Z., Zhang, X., and Liu, Y. (2022). Change point detection for high-dimensional linear models: A general tail-adaptive approach. *arXiv preprint arXiv:2207.11532*.
- Loh, P.-L. and Wainwright, M. J. (2012). High-dimensional regression with noisy and missing data: Provable guarantees with nonconvexity. *The Annals of Statistics*, 40(3):1637–1664.

- Maeng, H. and Fryzlewicz, P. (2019). Detecting linear trend changes in data sequences. *arXiv preprint arXiv:1906.01939*.
- Medeiros, M. C. and Mendes, E. F. (2016).  $\ell_1$ -regularization of high-dimensional time-series models with non-gaussian and heteroskedastic errors. *Journal of Econometrics*, 191.1 (2016):255–271.
- Messer, M., Kirchner, M., Schiemann, J., Roeper, J., Neining, R., and Schneider, G. (2014). A multiple filter test for the detection of rate changes in renewal processes with varying variance. *The Annals of Applied Statistics*, 8(4):2027–2067.
- Negahban, S. N., Ravikumar, P., Wainwright, M. J., and Yu, B. (2012). A unified framework for high-dimensional analysis of  $m$ -estimators with decomposable regularizers. *Statistical Science*, 27(4):538–557.
- Preuss, P., Puchstein, R., and Dette, H. (2015). Detection of multiple structural breaks in multivariate time series. *Journal of the American Statistical Association*, 110:654–668.
- Qu, Z. and Perron, P. (2007). Estimating and testing structural changes in multivariate regressions. *Econometrica*, 75(2):459–502.
- Rapach, D. E., Strauss, J. K., and Zhou, G. (2010). Out-of-sample equity premium prediction: Combination forecasts and links to the real economy. *The Review of Financial Studies*, 23(2):821–862.
- Rinaldo, A., Wang, D., Wen, Q., Willett, R., and Yu, Y. (2021). Localizing changes in high-dimensional regression models. In *International Conference on Artificial Intelligence and Statistics*, pages 2089–2097. PMLR.
- Serreze, M. C. and Meier, W. N. (2019). The arctic’s sea ice cover: trends, variability, predictability, and comparisons to the antarctic. *Annals of the New York Academy of Sciences*, 1436(1):36–53.
- Tibshirani, R. (1996). Regression shrinkage and selection via the lasso. *Journal of the Royal Statistical Society: Series B (Statistical Methodology)*, 58(1):267–288.
- Tibshirani, R. (2011). Regression shrinkage and selection via the lasso: a retrospective. *Journal of the Royal Statistical Society: Series B (Statistical Methodology)*, 73(3):273–282.
- van de Geer, S. A. and Bühlmann, P. (2009). On the conditions used to prove oracle results for the Lasso. *Electronic Journal of Statistics*, 3:1360–1392.
- Wang, D. and Zhao, Z. (2022). Optimal change-point testing for high-dimensional linear models with temporal dependence. *arXiv preprint arXiv:2205.03880*.
- Wang, D., Zhao, Z., Lin, K. Z., and Willett, R. (2021). Statistically and computationally efficient change point localization in regression settings. *Journal of Machine Learning Research*, 22(248):1–46.
- Wang, F., Madrid, O., Yu, Y., and Rinaldo, A. (2022). Denoising and change point localisation in piecewise-constant high-dimensional regression coefficients. In *International Conference on Artificial Intelligence and Statistics*, pages 4309–4338. PMLR.



- Welch, I. and Goyal, A. (2008). A comprehensive look at the empirical performance of equity premium prediction. *The Review of Financial Studies*, 21(4):1455–1508.
- Wong, K. C., Li, Z., and Tewari, A. (2020). Lasso guarantees for  $\beta$ -mixing heavy-tailed time series. *The Annals of Statistics*, 48(2):1124–1142.
- Wu, W. B. (2005). Nonlinear system theory: Another look at dependence. *Proceedings of the National Academy of Sciences*, 102(40):14150–14154.
- Wu, W. B. (2011). Asymptotic theory for stationary processes. *Statistics and its Interface*, 4(2):207–226.
- Xu, H., Wang, D., Zhao, Z., and Yu, Y. (2022). Change point inference in high-dimensional regression models under temporal dependence. *arXiv preprint arXiv:2207.12453*.
- Yau, C. Y. and Zhao, Z. (2016). Inference for multiple change points in time series via likelihood ratio scan statistics. *Journal of the Royal Statistical Society: Series B (Statistical Methodology)*, 78:895–916.
- Zhang, B., Geng, J., and Lai, L. (2015). Change-point estimation in high dimensional linear regression models via sparse group lasso. In *2015 53rd Annual Allerton Conference on Communication, Control, and Computing (Allerton)*, pages 815–821. IEEE.
- Zhang, D. and Wu, W. B. (2017). Gaussian approximation for high dimensional time series. *The Annals of Statistics*, 45(5):1895–1919.
- Zhang, D. and Wu, W. B. (2021). Convergence of covariance and spectral density estimates for high-dimensional locally stationary processes. *The Annals of Statistics*, 49(1):233–254.
- Zou, C., Wang, G., and Li, R. (2020). Consistent selection of the number of change-points via sample-splitting. *The Annals of statistics*, 48(1):413.

## A Literature review and comparison with the existing methods

Table A.7 provides an overview of the theoretical properties of data segmentation methods proposed in Wang et al. (2021), Kaul et al. (2019a) and Xu et al. (2022) for the change point problem in (1) under Gaussianity, and their computational complexity in comparison with those of MOSEG and MOSEG.MS. For a given methodology, let  $\hat{\mathcal{K}}$  denote the set of estimated change points. When the magnitude of change  $\Delta$ , measured by either  $\Delta^{(1)}$  defined in (10) or  $\Delta^{(2)}$  in (17) by taking into account both  $\delta_j$  and  $\min(\theta_j - \theta_{j-1}, \theta_{j+1} - \theta_j)$ , diverges faster than the separation rate  $s_{n,p}$  associated with the method, all  $q$  changes are detected by  $\hat{\mathcal{K}}$  with asymptotic power one and their locations are consistently estimated with the rate  $\ell_{n,p}$ , such that  $\min_{1 \leq j \leq q} \min_{\hat{k} \in \hat{\mathcal{K}}} w_j |\hat{k} - \theta_j| = O_P(\ell_{n,p})$ . Here,  $w_j$  refers to the relative difficulty in locating  $\theta_j$  which is related to the jump size  $\delta_j$ .

Table A.7: Comparison of data segmentation methods developed for the model (1) in their theoretical properties under Gaussianity and computational complexity. Here,  $\mathfrak{s} = \max_{0 \leq j \leq q} |\mathcal{S}_j|$  and  $\mathfrak{S} = |\cup_{j=0}^q \mathcal{S}_j|$ . See the text for the definitions of  $s_{n,p}$ ,  $\ell_{n,p}$ ,  $\Delta$  and  $w_j$ .

	Separation		Localisation		Computational
	$s_{n,p}$	$\Delta$	$\ell_{n,p}$	$w_j$	complexity
MOSEG	$\mathfrak{s} \log(pn)$	$\Delta^{(1)}$	$\mathfrak{s} \log(pn)$	$\delta_j$	$O(\frac{n}{rG} \cdot \text{Lasso}(G, p))$
MOSEG.MS	$\mathfrak{s} \log(pn)$	$\Delta^{(2)}$	$\mathfrak{s} \log(pn)$	$\delta_j$	$O(\frac{n}{rG_1} \cdot \text{Lasso}(n, p))$
Wang et al. (2021)	$\mathfrak{s} \log(pn)$	$\Delta^{(1)}$	$\mathfrak{s} \log(n)$	$\delta_j$	$O(n \log^2(n) \cdot \text{GroupLasso}(n, p))$
Kaul et al. (2019a)	$\mathfrak{S} \log(pn)$	$\Delta^{(1)}$	$\mathfrak{S} \log(p)$	$\delta$	$O(\tilde{q} \cdot \text{Lasso}(n, p) + \text{SA}(\tilde{q}))$
Xu et al. (2022)	$\mathfrak{s} \log(pn)$	$\Delta^{(1)}$	$\mathfrak{s} \log(pn)$	$\delta_j$	$O(n^2 \text{Lasso}(n, p))$

Wang et al. (2021) propose a method which learns the projection that is well-suited to reveal a change over each local segment and combines it with the wild binary segmentation algorithm (Fryzlewicz, 2014) for multiple change point detection.

Kaul et al. (2019a) propose to minimise an  $\ell_0$ -penalised cost function given a set of candidate estimators of size  $\tilde{q}$ . Their theoretical analysis implicitly assumes that  $\min_j(\theta_{j+1} - \theta_j)$  scales linearly in  $n$ , and the simulated annealing adopted for minimising the penalised cost, denoted by  $\text{SA}(\tilde{q})$  in Table A.7, has complexity ranging from  $O(\tilde{q}^4)$  on average to being exponential in the worst case.

Xu et al. (2022) investigate the dynamic programming algorithm of Rinaldo et al. (2021) for minimising a  $\ell_0$ -penalised cost function in a more general setting. In Table A.7, we report the separation and localisation rates derived in Xu et al. (2022) for the pre-estimators from the dynamic programming algorithm; in their proposal, the pre-estimators are further refined and their exact minimax optimality is established under a stronger condition on the size of changes, namely that  $\Delta^{(1)}/(\mathfrak{s}^2 \log^3(pn)) \rightarrow \infty$ .

We also mention Zhang et al. (2015) where the data segmentation problem is treated as a high-dimensional regression problem with a group Lasso penalty, which only provides that the

estimation bias is of  $o_P(n)$ . Leonardi and Bühlmann (2016) consider both dynamic programming and binary segmentation algorithms are considered for change point estimation, and we refer to Rinaldo et al. (2021) for a detailed discussion on their results.

From Table A.7, we conclude that MOSEG.MS is highly competitive both computationally and statistically. In specifying the properties of Kaul et al. (2019a), the global sparsity  $\mathfrak{S} = |\cup_{j=0}^q \mathcal{S}_j|$  can be much greater than the segment-wise sparsity  $\mathfrak{s}$ , particularly when the number of change points  $q$  is large. We investigate the theoretical properties of MOSEG.MS in the broadest parameter space possible which is formulated with  $\Delta^{(2)}$  instead of  $\Delta^{(1)}$  as in all the other papers (see also the discussion following (17) comparing  $\Delta^{(l)}$ ,  $l = 1, 2$ ). Besides, the theoretical properties of MOSEG.MS reported in Table A.7 do not require independence unlike other works (with the exception of Xu et al. (2022)), and extend beyond i.i.d. sub-Gaussianity.

## B Additional simulations

### B.1 Choice of the grid

We compare the change point estimators obtained in Stages 1 and 2 of MOSEG when the finest grid ( $r = G^{-1}$ ) and a coarse grid ( $r = 1/10$ )  $\mathcal{T}(r, G)$  are used in Stage 1, see (5). For this, we set  $n = 300$ ,  $p = 100$ ,  $\mathfrak{s} = 2$  and  $q = 1$ , and randomly generate  $\mathbf{x}_t \sim_{\text{iid}} \mathcal{N}_p(\mathbf{0}, \mathbf{I})$  and  $\varepsilon_t \sim_{\text{iid}} \mathcal{N}(0, 1)$ . The change point  $\theta_1$  is randomly sampled from  $\{51, \dots, 250\}$  and varying  $\delta \in \{0.1, 0.2, 0.4, 0.8\}$ , we generate  $\boldsymbol{\beta}_0 = (\beta_{0,1}, \dots, \beta_{0,p})^\top$  with  $\beta_{0,i} = \delta \cdot (-1)^{i-1}$  for  $i \in \{1, \dots, \mathfrak{s}\}$  and have  $\boldsymbol{\beta}_1 = -\boldsymbol{\beta}_0$ . Using  $G = 50$ , we select the maximiser of the MOSUM statistic as the initial estimator  $\tilde{\theta}_1$ , which then is refined as in (9). Table B.1 reports the average and the standard error of  $n^{-1}|\tilde{\theta}_1 - \theta_1|$  (from Stage 1) and  $n^{-1}|\hat{\theta}_1 - \theta_1|$  (from Stage 2) over 100 realisations when different grids are used. We observe that regardless of the coarseness of the grid, the refinement step performed in Stage 2 improves the localisation performance. At the same time, there is little loss in estimation accuracy attributable to the increasing coarseness of the grid regardless of  $\delta$ .

Table B.1: Comparison of  $d_H$  for Stage 1 and Stage 2 estimators from MOSEG when different grids are used. The average and the standard error of estimation errors over 100 realisations are reported.

$\delta$	$r = G^{-1}$				$r = 1/10$			
	Stage 1		Stage 2		Stage 1		Stage 2	
	Mean	SD	Mean	SD	Mean	SD	Mean	SD
0.1	0.2197	0.1597	0.2141	0.1655	0.2238	0.1447	0.2153	0.1484
0.2	0.1795	0.1622	0.1472	0.1712	0.1876	0.1767	0.1696	0.1770
0.4	0.0102	0.0133	0.0045	0.0073	0.0135	0.0212	0.0053	0.0101
0.8	0.0053	0.0051	0.0010	0.0018	0.0072	0.0080	0.0010	0.0017

## B.2 Heavy-tailedness and temporal dependence

We examine the performance of MOSEG.MS in the presence of heavy-tailed noise and temporal dependence. For this, we generate datasets with  $n = 300$ ,  $p = 100$ ,  $\mathfrak{s}, q = 1$  and the two change points are located at  $\theta_j = jn/3$ ,  $j = 1, 2$ . We use  $\beta_0$  obtained as in Appendix B.1 and set  $\beta_j = (-1)^j \cdot \beta_0$ . MOSEG.MS is applied with the recommended bandwidth set and the CV-based model selection discussed in Section 4.1. We consider the following three settings for the generation of  $\mathbf{x}_t$  and  $\varepsilon_t$ .

(E1)  $\mathbf{x}_t \sim_{\text{iid}} \mathcal{N}_p(\mathbf{0}, \mathbf{I})$  and  $\varepsilon_t \sim_{\text{iid}} \mathcal{N}(0, 1)$  for all  $t$ .

(E2)  $X_{it} \sim_{\text{iid}} \sqrt{3/5} \cdot t_5$  for all  $i$  and  $t$  and  $\varepsilon_t \sim_{\text{iid}} \sqrt{3/5} \cdot t_5$  for all  $t$ .

(E3)  $\{(\mathbf{x}_t, \varepsilon_t)\}_{t=1}^n$  is generated as in (12) where  $\mathbf{D}_1$  is a diagonal matrix with 0.3 on its diagonals,  $\mathbf{D}_\ell = \mathbf{O}$  for  $\ell \geq 2$  and  $\zeta_t \sim_{\text{iid}} \mathcal{N}_{p+1}(\mathbf{0}, \sqrt{1 - 0.3^2} \mathbf{I})$  for all  $t$ .

Under (E2)–(E3), the data is permitted to be heavy-tailed and serially correlated, respectively; (E1) serves as a benchmark. Table B.2 reports the average and standard error of the Hausdorff distance in (19) and  $\hat{q} - q$  over 100 realisations. It shows that generally, MOSEG.MS is not sensitive to heavy-tailedness or temporal dependence.

Table B.2: Performance of MOSEG.MS under (E1)–(E3) over 100 realisations.

$\delta$	Setting	$\hat{q} - q$						$d_H$	
		-2	-1	0	1	2	$\geq 3$	Mean	SD
1	(E1)	0	1	98	1	0	0	0.0078	0.0348
	(E2)	0	2	96	2	0	0	0.0105	0.0460
	(E3)	0	0	99	1	0	0	0.0058	0.0174
1.2	(E1)	0	0	98	2	0	0	0.0038	0.0111
	(E2)	0	0	99	1	0	0	0.0027	0.0077
	(E3)	0	0	97	3	0	0	0.0055	0.0141
1.4	(E1)	0	0	97	3	0	0	0.0047	0.0134
	(E2)	0	0	99	1	0	0	0.0036	0.0111
	(E3)	0	0	98	2	0	0	0.0040	0.0125
1.6	(E1)	0	0	99	1	0	0	0.0031	0.0076
	(E2)	0	0	99	1	0	0	0.0019	0.0044
	(E3)	0	0	97	3	0	0	0.0055	0.0197

## C Proofs

In what follows, for any vector  $\mathbf{a} \in \mathbb{R}^p$  and a set  $\mathcal{A} \subset \{1, \dots, p\}$ , we denote by  $\mathbf{a}(\mathcal{A}) = (a_i, i \in \mathcal{A})^\top$  the sub-vector of  $\mathbf{a}$  supported on  $\mathcal{A}$ . We write the population counterpart of  $T_k(G)$  with  $\beta_{s,e}^*$  defined in (4) as

$$T_k^*(G) = \sqrt{\frac{G}{2}} |\beta_{k,k+G}^* - \beta_{k-G,k}^*|_2.$$

Further, we write  $\mathcal{S}_{s,e} = \text{supp}(\boldsymbol{\beta}_{s,e}^*)$ .

## C.1 Proof of Theorem 1

### C.1.1 Supporting lemmas

**Lemma C.1.** We have

$$T_k^*(G) = \begin{cases} \frac{1}{\sqrt{2G}}(G - |k - \theta_j|)\delta_j & \text{if } \{k - G + 1, \dots, k + G\} \cap \Theta = \{\theta_j\}, \\ 0 & \text{if } \{k - G + 1, \dots, k + G\} \cap \Theta = \emptyset \end{cases}$$

**Lemma C.2.** Define  $\boldsymbol{\Delta}_{s,e} = \widehat{\boldsymbol{\beta}}_{s,e} - \boldsymbol{\beta}_{s,e}^*$ . With  $\lambda \geq 4C_{\text{DEV}}\rho_{n,p}$ , we have  $\mathbb{P}(\mathcal{B}) \geq 1 - \mathbb{P}(\mathcal{R}^{(1)} \cap \mathcal{D}^{(2)})$  where

$$\mathcal{B} = \left\{ |\boldsymbol{\Delta}_{s,e}|_2 \leq \frac{12\sqrt{2s}\lambda}{\omega\sqrt{e-s}} \text{ and } |\boldsymbol{\Delta}_{s,e}(\mathcal{S}_{s,e}^c)|_1 \leq 3|\boldsymbol{\Delta}_{s,e}(\mathcal{S}_{s,e})|_1 \text{ for all } 0 \leq s < e \leq n \right. \\ \left. \text{with } |\{s+1, \dots, e\} \cap \Theta| \leq 1 \text{ and } e-s \geq C_0 \max \left[ (\omega^{-1}s \log(p))^{\frac{1}{1-\tau}}, \rho_{n,p}^2 \right] \right\}.$$

*Proof.* For given  $0 \leq s < e \leq n$ , we have

$$\sum_{t=s+1}^e \left( Y_t - \mathbf{x}_t^\top \widehat{\boldsymbol{\beta}}_{s,e} \right)^2 + \lambda \sqrt{e-s} |\widehat{\boldsymbol{\beta}}_{s,e}|_1 \leq \sum_{t=s+1}^e \left( Y_t - \mathbf{x}_t^\top \boldsymbol{\beta}_{s,e}^* \right)^2 + \lambda \sqrt{e-s} |\boldsymbol{\beta}_{s,e}^*|_1,$$

from which it follows that

$$\lambda \sqrt{e-s} \left( |\boldsymbol{\beta}_{s,e}^*|_1 - |\widehat{\boldsymbol{\beta}}_{s,e}|_1 \right) \geq \sum_{t=s+1}^e \left[ (\mathbf{x}_t^\top \widehat{\boldsymbol{\beta}}_{s,e})^2 - (\mathbf{x}_t^\top \boldsymbol{\beta}_{s,e}^*)^2 - 2Y_t \mathbf{x}_t^\top (\widehat{\boldsymbol{\beta}}_{s,e} - \boldsymbol{\beta}_{s,e}^*) \right] \\ y = \sum_{t=s+1}^e \left[ \boldsymbol{\Delta}_{s,e}^\top \mathbf{x}_t \mathbf{x}_t^\top \boldsymbol{\Delta}_{s,e} - 2(Y_t - \mathbf{x}_t^\top \boldsymbol{\beta}_{s,e}^*) \mathbf{x}_t^\top \boldsymbol{\Delta}_{s,e} \right].$$

Then, noting that  $\boldsymbol{\beta}_{s,e}^*(\mathcal{S}_{s,e}^c) = \mathbf{0}$ ,

$$\frac{1}{\sqrt{e-s}} \sum_{t=s+1}^e \left[ \boldsymbol{\Delta}_{s,e}^\top \mathbf{x}_t \mathbf{x}_t^\top \boldsymbol{\Delta}_{s,e} - 2(Y_t - \mathbf{x}_t^\top \boldsymbol{\beta}_{s,e}^*) \mathbf{x}_t^\top \boldsymbol{\Delta}_{s,e} \right] + \lambda |\widehat{\boldsymbol{\beta}}_{s,e}(\mathcal{S}_{s,e}^c)|_1 \\ \leq \lambda \left( |\boldsymbol{\beta}_{s,e}^*(\mathcal{S}_{s,e})|_1 - |\widehat{\boldsymbol{\beta}}_{s,e}(\mathcal{S}_{s,e})|_1 \right) \leq \lambda |\boldsymbol{\Delta}_{s,e}(\mathcal{S}_{s,e})|_1. \quad (\text{C.1})$$

Since  $\lambda \geq 4C_{\text{DEV}}\rho_{n,p}$ , it follows from (C.1) that on  $\mathcal{D}^{(2)}$ ,

$$\frac{1}{\sqrt{e-s}} \sum_{t=s+1}^e \boldsymbol{\Delta}_{s,e}^\top \mathbf{x}_t \mathbf{x}_t^\top \boldsymbol{\Delta}_{s,e} - \frac{\lambda}{2} |\boldsymbol{\Delta}_{s,e}|_1 + \lambda |\boldsymbol{\Delta}_{s,e}(\mathcal{S}_{s,e}^c)|_1 \leq \lambda |\boldsymbol{\Delta}_{s,e}(\mathcal{S}_{s,e})|_1,$$

$$\therefore 0 \leq \frac{1}{\sqrt{e-s}} \sum_{t=s+1}^e \Delta_{s,e}^\top \mathbf{x}_t \mathbf{x}_t^\top \Delta_{s,e} \leq \frac{\lambda}{2} \left( 3 |\Delta_{s,e}(\mathcal{S}_{s,e})|_1 - |\Delta_{s,e}(\mathcal{S}_{s,e}^c)|_1 \right),$$

such that

$$|\Delta_{s,e}(\mathcal{S}_{s,e}^c)|_1 \leq 3 |\Delta_{s,e}(\mathcal{S}_{s,e})|_1. \quad (\text{C.2})$$

This in particular leads to

$$|\Delta_{s,e}|_1 \leq 4 |\Delta_{s,e}(\mathcal{S}_{s,e})|_1 \leq 4\sqrt{2\mathfrak{s}} |\Delta_{s,e}|_2$$

from the definition of  $\mathfrak{s}$ . Then on  $\mathcal{R}^{(1)}$ , we have

$$\begin{aligned} 6\sqrt{2\mathfrak{s}}\lambda |\Delta_{s,e}|_2 &\geq \frac{1}{\sqrt{e-s}} \sum_{t=s+1}^e \Delta_{s,e}^\top \mathbf{x}_t \mathbf{x}_t^\top \Delta_{s,e} \\ &\geq \omega \sqrt{e-s} |\Delta_{s,e}|_2^2 - \frac{32C_{\text{RSC}}\mathfrak{s} \log(p)(e-s)^\tau}{\sqrt{e-s}} |\Delta_{s,e}|_2^2 \geq \frac{\omega}{2} \sqrt{e-s} |\Delta_{s,e}|_2^2, \end{aligned}$$

where the last inequality follows for  $(e-s)^{1-\tau} \geq 64C_{\text{RSC}}\omega^{-1}\mathfrak{s} \log(p)$ . In summary,

$$|\Delta_{s,e}|_2 \leq \frac{12\sqrt{2\mathfrak{s}}\lambda}{\omega \sqrt{e-s}}. \quad (\text{C.3})$$

Combining (C.2) and (C.3), the proof is complete.  $\square$

### C.1.2 Proof of Theorem 1 (i)

Let  $\mathcal{T}_j = \{\theta_j - \lfloor \eta G \rfloor + 1, \dots, \theta_j + \lfloor \eta G \rfloor\} \cap \mathcal{T}$  for  $1 \leq j \leq q$ . Under Assumptions 4 and 5, we have  $G \geq C_\delta^{-2} C_1 \max\{\omega^{-2}\mathfrak{s}\rho_{n,p}^2, (\omega^{-1}\mathfrak{s} \log(p))^{1/(1-\tau)}\}$  such that the lower bound on  $(e-s)$  made in  $\mathcal{B}$  (see Lemma C.2) is met by all  $s = k$  and  $e = k + G$ ,  $k = 0, \dots, n - G$ . By Lemma C.2,

$$\begin{aligned} \max_{G \leq k \leq n-G} |T_k(G) - T_k^*(G)| &\leq \\ \max_{G \leq k \leq n-G} \sqrt{\frac{G}{2}} \left( \left| \hat{\beta}_{k-G,k} - \beta_{k-G,k}^* \right|_2 + \left| \hat{\beta}_{k,k+G} - \beta_{k,k+G}^* \right|_2 \right) &\leq \frac{24\sqrt{\mathfrak{s}}\lambda}{\omega}. \end{aligned} \quad (\text{C.4})$$

First, consider some  $k$  for which  $\{k - G + 2, \dots, k + G - 1\} \cap \Theta = \emptyset$ . Then, we have  $T_k^*(G) = 0$  from Lemma C.1 such that by (C.4),

$$\max_{k: \min_{1 \leq j \leq q} |k - \theta_j| \geq G} T_k(G) \leq \max_{G \leq \ell \leq n-G} |T_\ell(G) - T_\ell^*(G)| \leq \frac{24\sqrt{\mathfrak{s}}\lambda}{\omega} \leq D. \quad (\text{C.5})$$

This ensures that any  $\tilde{\theta} \in \tilde{\Theta}$  satisfies  $\min_{1 \leq j \leq q} |\tilde{\theta} - \theta_j| < G$ . Next, let  $\theta_j^L$  and  $\theta_j^R$  denote two points within  $\mathcal{T}_j$  which are the closest to  $\theta_j$  from the left and the right of  $\theta_j$ , respectively,

with  $\theta_j^L = \theta_j^R$  when  $r = 1/G$ . Then by construction of  $\mathcal{T}$ ,

$$\max(k_j - \theta_j^L, \theta_j^R - \theta_j) \leq \lfloor rG \rfloor \quad \text{and} \quad \min(\theta_j - \theta_j^L, \theta_j^R - \theta_j) \leq \frac{\lfloor rG \rfloor}{2}, \quad (\text{C.6})$$

such that from Lemma C.1,

$$\max\left(T_{\theta_j^L}^*(G), T_{\theta_j^R}^*(G)\right) \geq \frac{\delta_j(G - \lfloor rG \rfloor/2)}{\sqrt{2G}} \geq \sqrt{\frac{G}{2}} \delta_j(1 - r/2).$$

From this and by (C.4), at  $\tilde{\theta}_j = \arg \max_{k \in \mathcal{T}_j} T_k(G)$ , we have

$$T_{\tilde{\theta}_j}(G) \geq \max\left(T_{\theta_j^L}(G), T_{\theta_j^R}(G)\right) \geq \sqrt{\frac{G}{2}} \delta_j \left(1 - \frac{r}{2}\right) - \frac{24\sqrt{5}\lambda}{\omega} > \frac{1 - r/2}{2} \sqrt{\frac{G}{2}} \delta_j > D,$$

where the second last inequality follows from Assumption 5 (b), and the last one from (11).

When  $\eta = 1$ , this and (C.5) indicates that such  $\tilde{\theta}_j$  satisfies (6). When  $\eta < 1$ , note that

$$\begin{aligned} & \max\left(T_{\theta_j^L}(G), T_{\theta_j^R}(G)\right) - \max\{T_k(G) : |k - \theta_j| > (1 - \eta)G, k \in \mathcal{T}\} \\ & \geq \sqrt{\frac{G}{2}} \delta_j \left(\eta - \frac{3r}{2}\right) - \frac{48\sqrt{5}\lambda}{\omega} \geq \frac{5\eta}{8\sqrt{2}} \min_{1 \leq j \leq q} \delta_j \sqrt{G} - \frac{48\sqrt{5}\lambda}{\omega} > 0 \end{aligned}$$

from (11). These arguments ensure that we detect at least one change point in  $\mathcal{T}_j$  at  $t = \tilde{\theta}_j$  for each  $j = 1, \dots, q$ . For such  $\tilde{\theta}_j$ , suppose that  $\theta_j^\circ = \arg \min_{k \in \{\theta_j^L, \theta_j^R\}} |\tilde{\theta}_j - k|$ . Then,

$$\frac{\delta_j}{\sqrt{2G}}(G - |\tilde{\theta}_j - \theta_j|) + \frac{24\sqrt{5}\lambda}{\omega} \geq T_{\tilde{\theta}_j}(G) \geq T_{\theta_j^\circ}(G) \geq \frac{\delta_j}{\sqrt{2G}}(G - |\theta_j^\circ - \theta_j|) - \frac{24\sqrt{5}\lambda}{\omega}$$

and re-arranging, we obtain

$$\frac{\delta_j}{\sqrt{2G}} \left(|\tilde{\theta}_j - \theta_j| - |\theta_j^\circ - \theta_j|\right) \leq \frac{48\sqrt{5}\lambda}{\omega}, \text{ such that } |\tilde{\theta}_j - \theta_j| \leq \frac{48\sqrt{25G}\lambda}{\omega\delta_j} + \lfloor rG \rfloor < \left\lfloor \frac{G}{2} \right\rfloor,$$

for large enough  $C_1$  in Assumption 5 (b).

Finally, let  $\mathcal{L}_{\mathcal{T}}(t)$  denote the largest time point  $k' \in \mathcal{T}$  that satisfies  $k' \leq t$ , and define  $\mathcal{R}_{\mathcal{T}}(t)$  analogously. Then, we establish that

$$T_{\mathcal{L}_{\mathcal{T}}(\theta_j - \frac{\eta G}{2}m)}(G) > \max\left\{T_k(G) : \frac{\eta G}{2}(m+1) \leq \theta_j - k \leq \frac{\eta G}{2}(m+2), k \in \mathcal{T}\right\}, \quad (\text{C.7})$$

$$T_{\mathcal{R}_{\mathcal{T}}(\theta_j + \frac{\eta G}{2}m)}(G) > \max\left\{T_k(G) : \frac{\eta G}{2}(m+1) \leq k - \theta_j \leq \frac{\eta G}{2}(m+2), k \in \mathcal{T}\right\}, \quad (\text{C.8})$$

for  $m = 0, \dots, \lceil 2/\eta \rceil - 2$ . The inequality in (C.7) follows from noting that

$$\begin{aligned} T_{\mathcal{L}_{\mathcal{T}}(\theta_j - \frac{\eta G}{2} m)}(G) &= \max \left\{ T_k(G) : \frac{\eta G}{2}(m+1) \leq \theta_j - k \leq \frac{\eta G}{2}(m+2), k \in \mathcal{T} \right\} \\ &\geq \sqrt{\frac{G}{2}} \delta_j \left( \frac{\eta}{2} - r \right) - \frac{48\sqrt{\mathfrak{s}}\lambda}{\omega} \geq \frac{\eta}{4\sqrt{2}} \min_{1 \leq j \leq q} \delta_j \sqrt{G} - \frac{48\sqrt{\mathfrak{s}}\lambda}{\omega} > 0 \end{aligned}$$

under (11), and the inequality in (C.8) follows analogously. This ensures that  $\tilde{\theta}_j$  by its construction is the unique local maximiser of  $T_k(G)$  within the interval  $\{\theta_j - G + 1, \dots, \theta_j + G\} \cap \mathcal{T}$  satisfying (6) for each  $j = 1, \dots, q$ , which completes the proof.

### C.1.3 Proof of Theorem 1 (ii)

Recalling (7), we write

$$Q_j(k) = \sum_{t=\tilde{\theta}_j-G+1}^k (Y_t - \mathbf{x}_t^\top \hat{\boldsymbol{\beta}}_j^L)^2 + \sum_{t=k+1}^{\tilde{\theta}_j+G} (Y_t - \mathbf{x}_t^\top \hat{\boldsymbol{\beta}}_j^R)^2.$$

Theorem 1 (i) establishes that for each  $j = 1, \dots, q$ , we have  $\tilde{\theta}_j \in \tilde{\Theta}$  that satisfies  $|\tilde{\theta}_j - \theta_j| < G/2$ , and  $\tilde{\Theta}$  contains no other estimator. Then under Assumption 5 (a), we have the following statements satisfied for all  $j$ .

- (i) Defining  $\mathcal{I}(\tilde{\theta}_j) = \{\tilde{\theta}_j - G + 1, \dots, \tilde{\theta}_j + G\}$ , it fulfils  $\mathcal{I}(\tilde{\theta}_j) \cap \Theta = \{\theta_j\}$ .
- (ii)  $\{\tilde{\theta}_j^L - G + 1, \dots, \tilde{\theta}_j^L\} \subset \{\theta_{j-1} + 1, \dots, \theta_j\}$  and  $\{\tilde{\theta}_j^R + 1, \dots, \tilde{\theta}_j^R + G\} \subset \{\theta_j + 1, \dots, \theta_{j+1}\}$ , such that denoting by  $\boldsymbol{\Delta}_j^L = \hat{\boldsymbol{\beta}}_j^L - \boldsymbol{\beta}_{j-1}$  and  $\boldsymbol{\Delta}_j^R = \hat{\boldsymbol{\beta}}_j^R - \boldsymbol{\beta}_j$ , we have

$$\begin{aligned} \max \left( |\boldsymbol{\Delta}_j^L|_2, |\boldsymbol{\Delta}_j^R|_2 \right) &\leq \frac{12\sqrt{2\mathfrak{s}}\lambda}{\omega\sqrt{G}}, \\ |\boldsymbol{\Delta}_j^L(\mathcal{S}_{j-1}^c)|_1 &\leq 3 |\boldsymbol{\Delta}_j^L(\mathcal{S}_{j-1})|_1 \quad \text{and} \quad |\boldsymbol{\Delta}_j^R(\mathcal{S}_j^c)|_1 \leq 3 |\boldsymbol{\Delta}_j^R(\mathcal{S}_j)|_1 \end{aligned} \quad (\text{C.9})$$

in  $\mathcal{B}$ , see Lemma C.2.

Then we show that for all  $k \in \mathcal{I}(\tilde{\theta}_j)$  satisfying  $\delta_j^2 |k - \theta_j| > v_{n,p}$  with

$$v_{n,p} = \max \left( \mathfrak{s} \rho_{n,p}^2, (\mathfrak{s} \log(p))^{\frac{1}{1-\tau}} \right) \cdot \max \left\{ C_\delta^2 \max \left[ \frac{9C_{\text{RSC}}}{2\omega}, \frac{32C_{\text{RSC}}}{\bar{\omega}} \right]^{\frac{1}{1-\tau}}, \left( \frac{96C_{\text{DEV}}}{\omega} \right)^2 \right\}, \quad (\text{C.10})$$

we have  $Q_j(k) - Q_j(\theta_j) > 0$ , which completes the proof.



First, suppose that  $k \geq \theta_j + 1$ . Then,

$$\begin{aligned}
Q_j(k) - Q_j(\theta_j) &= \sum_{t=\theta_j+1}^k \left[ (Y_t - \mathbf{x}_t^\top \hat{\boldsymbol{\beta}}_j^L)^2 - (Y_t - \mathbf{x}_t^\top \hat{\boldsymbol{\beta}}_j^R)^2 \right] \\
&= \sum_{t=\theta_j+1}^k (\boldsymbol{\beta}_j - \hat{\boldsymbol{\beta}}_j^L)^\top \mathbf{x}_t \mathbf{x}_t^\top (\boldsymbol{\beta}_j - \hat{\boldsymbol{\beta}}_j^L) - \sum_{t=\theta_j+1}^k (\hat{\boldsymbol{\beta}}_j^R - \boldsymbol{\beta}_j)^\top \mathbf{x}_t \mathbf{x}_t^\top (\hat{\boldsymbol{\beta}}_j^R - \boldsymbol{\beta}_j) \\
&\quad + 2 \sum_{t=\theta_j+1}^k \varepsilon_t \mathbf{x}_t^\top \left[ (\boldsymbol{\beta}_j - \boldsymbol{\beta}_{j-1}) + (\hat{\boldsymbol{\beta}}_j^R - \boldsymbol{\beta}_j) - (\hat{\boldsymbol{\beta}}_j^L - \boldsymbol{\beta}_{j-1}) \right] = I_1 + I_2 + I_3.
\end{aligned}$$

From the definition of  $\mathfrak{s}$  and the Cauchy-Schwarz inequality,

$$|\boldsymbol{\beta}_j - \boldsymbol{\beta}_{j-1}|_1 \leq \sqrt{2\mathfrak{s}} |\boldsymbol{\beta}_j - \boldsymbol{\beta}_{j-1}|_2 \quad (\text{C.11})$$

and from (C.9), we have

$$|\boldsymbol{\Delta}_j^L|_1 \leq 4|\boldsymbol{\Delta}_j^L(\mathcal{S}_j)|_1 \leq 4\sqrt{2\mathfrak{s}} |\boldsymbol{\Delta}_j^L|_2 \text{ and analogously, } |\boldsymbol{\Delta}_j^R|_1 \leq 4\sqrt{2\mathfrak{s}} |\boldsymbol{\Delta}_j^R|_2. \quad (\text{C.12})$$

From (C.11)–(C.12), we derive

$$\begin{aligned}
|\hat{\boldsymbol{\beta}}_j^L - \boldsymbol{\beta}_j|_2 &\leq \delta_j \left( 1 + \frac{12\sqrt{2\mathfrak{s}}\lambda}{\omega\delta_j\sqrt{G}} \right) \leq \frac{3\delta_j}{2} \text{ and similarly, } |\hat{\boldsymbol{\beta}}_j^L - \boldsymbol{\beta}_j|_2 \geq \frac{\delta_j}{2}, \\
|\hat{\boldsymbol{\beta}}_j^L - \boldsymbol{\beta}_j|_1 &\leq \sqrt{\mathfrak{s}}\delta_j \left( 1 + \frac{96\sqrt{\mathfrak{s}}\lambda}{\omega\delta_j\sqrt{G}} \right) \leq \frac{3\sqrt{\mathfrak{s}}\delta_j}{2},
\end{aligned}$$

for a large enough  $C_1$  in Assumption 5 (b). Then on  $\mathcal{R}^{(1)}$ , we have

$$I_1 \geq |k - \theta_j| \omega \delta_j^2 \left( \frac{1}{4} - \frac{9C_{\text{RSC}}\mathfrak{s} \log(p)}{4|k - \theta_j|^{1-\tau}\omega} \right) \geq \frac{\omega}{8} \delta_j^2 |k - \theta_j| \quad (\text{C.13})$$

from that  $|k - \theta_j| > \delta_j^{-2} v_{n,p} \geq C_\delta^{-2} v_{n,p}$  (from Assumption 4) and (C.10). As for  $I_2$ , from Lemma C.2, (C.10) and (C.12) we have on  $\mathcal{R}^{(2)}$ ,

$$|I_2| \leq |\boldsymbol{\Delta}_j^R|_2^2 [|k - \theta_j| \bar{\omega} + 32C_{\text{RSC}}\mathfrak{s} \log(p) |k - \theta_j|^\tau] \leq 2|k - \theta_j| \bar{\omega} |\boldsymbol{\Delta}_j^R|_2^2 \leq \frac{576\bar{\omega}\mathfrak{s} |k - \theta_j| \lambda^2}{\omega^2 G}. \quad (\text{C.14})$$

Turning our attention to  $I_3$ , from (C.11)–(C.12),

$$\begin{aligned}
|(\boldsymbol{\beta}_j - \boldsymbol{\beta}_{j-1}) + (\hat{\boldsymbol{\beta}}_j^R - \boldsymbol{\beta}_j) - (\hat{\boldsymbol{\beta}}_j^L - \boldsymbol{\beta}_{j-1})|_1 &\leq |\boldsymbol{\beta}_j - \boldsymbol{\beta}_{j-1}|_1 + |\hat{\boldsymbol{\beta}}_j^R - \boldsymbol{\beta}_j|_1 + |\hat{\boldsymbol{\beta}}_j^L - \boldsymbol{\beta}_{j-1}|_1 \\
&\leq \sqrt{\mathfrak{s}}\delta_j \left( 1 + \frac{192\sqrt{\mathfrak{s}}\lambda}{\omega\delta_j\sqrt{G}} \right) \leq 2\sqrt{\mathfrak{s}}\delta_j,
\end{aligned}$$

where the last inequality follows from Assumption 5 (b). Then on  $\mathcal{D}^{(1)}$ ,

$$\begin{aligned} \frac{1}{2}|I_3| &\leq \left| \sum_{t=\theta_j+1}^k \varepsilon_t \mathbf{x}_t^\top \right|_\infty \left| (\boldsymbol{\beta}_j - \boldsymbol{\beta}_{j-1}) + (\widehat{\boldsymbol{\beta}}_j^{\text{R}} - \boldsymbol{\beta}_j) - (\widehat{\boldsymbol{\beta}}_j^{\text{L}} - \boldsymbol{\beta}_{j-1}) \right|_1 \\ &\leq 2C_{\text{DEV}} \delta_j \sqrt{\mathfrak{s}(k - \theta_j)} \rho_{n,p}. \end{aligned} \quad (\text{C.15})$$

Then from (C.13), (C.14) and (C.15), we derive

$$\frac{|I_2|}{I_1} = \frac{4608\bar{\omega}\mathfrak{s}\lambda^2}{\omega^3\delta_j^2 G} \leq \frac{1}{3} \quad \text{and} \quad \frac{|I_3|}{I_1} = \frac{32C_{\text{DEV}}\sqrt{\mathfrak{s}}\rho_{n,p}}{\omega\delta_j\sqrt{k - \theta_j}} \leq \frac{1}{3}$$

under Assumption 5 (b), for all  $k \in \mathcal{I}_j$  satisfying  $\delta_j^2|k - \theta_j| > v_{n,p}$  from (C.10). Analogous arguments apply when  $k \leq \theta_j$ , and the above arguments are deterministic on  $\mathcal{M}$ . In summary, we have

$$\min_{1 \leq j \leq q} \min_{\substack{k \in \mathcal{I}_j \\ \delta_j^2|k - \theta_j| > v_{n,p}}} (Q_j(k) - Q_j(\theta_j)) > \frac{\omega}{24} v_{n,p} > 0,$$

which concludes the proof.

## C.2 Proof of Proposition 2

### C.2.1 Supporting lemmas

Define  $\mathbb{K}(b) = \mathbb{B}_0(b) \cap \mathbb{B}_1(1)$  with some  $b \geq 1$ , where  $\mathbb{B}_d(r) = \{\mathbf{a} : |\mathbf{a}|_d \leq r\}$  with the dimension of  $\mathbf{a}$  determined within the context. Let  $\mathbf{e}_i$  denote a vector that contains zeros except for its  $i$ th component set to be one. We denote the time-varying vector of parameters under (1) by  $\boldsymbol{\beta}(t) = \sum_{j=1}^{q+1} \boldsymbol{\beta}_j \mathbb{I}_{\{\theta_{j-1}+1 \leq t \leq \theta_j\}}$ .

Denote by  $\mathbf{Z}_t = (\mathbf{x}_t^\top, \varepsilon_t)^\top \in \mathbb{R}^{p+1}$  which admits  $\mathbf{Z}_t = \sum_{\ell=0}^{\infty} \mathbf{D}_\ell \boldsymbol{\xi}_{t-\ell}$  under (12). For some  $\mathbf{a}, \mathbf{b} \in \mathbb{B}_2(1)$ , define  $U_t(\mathbf{a}) = \mathbf{a}^\top \mathbf{Z}_t$  and  $W_t(\mathbf{a}, \mathbf{b}) = \mathbf{a}^\top \mathbf{Z}_t \mathbf{Z}_t^\top \mathbf{b}$ . Let  $\boldsymbol{\xi}'_t$  denote an independent copy of  $\boldsymbol{\xi}_t$ , and define  $\mathbf{Z}_{t,\{0\}} = \sum_{\ell=0, \ell \neq t}^{\infty} \mathbf{D}_\ell \boldsymbol{\xi}_{t-\ell} + \mathbf{D}_t \boldsymbol{\xi}'_0$ . We denote the functional dependence measure and the dependence-adjusted norm for  $U_t(\mathbf{a})$  as defined in Zhang and Wu (2017), by

$$\delta_{t,\nu}(\mathbf{a}) = \left\| \mathbf{a}^\top \mathbf{Z}_t - \mathbf{a}^\top \mathbf{Z}_{t,\{0\}} \right\|_\nu \quad \text{and} \quad \lll U.(\mathbf{a}) \rrr_\nu = \sum_{t=0}^{\infty} \delta_{t,\nu}(\mathbf{a}),$$

respectively. Analogously, we define

$$\delta_{t,\nu}(\mathbf{a}, \mathbf{b}) = \left\| \mathbf{a}^\top \mathbf{Z}_t \mathbf{Z}_t^\top \mathbf{b} - \mathbf{a}^\top \mathbf{Z}_{t,\{0\}} \mathbf{Z}_{t,\{0\}}^\top \mathbf{b} \right\|_\nu \quad \text{and} \quad \lll W.(\mathbf{a}, \mathbf{b}) \rrr_\nu = \sum_{t=0}^{\infty} \delta_{t,\nu}(\mathbf{a}, \mathbf{b})$$

for  $W_t(\mathbf{a}, \mathbf{b})$ . Finally, for some  $\kappa \geq 0$ , we denote the dependence adjusted sub-exponential

norm of  $W_t(\mathbf{a}, \mathbf{b})$  by  $\|W_t(\mathbf{a}, \mathbf{b})\|_{\psi_\kappa} = \sup_{\nu \geq 2} \nu^{-\kappa} \|W_t(\mathbf{a}, \mathbf{b})\|_\nu$ . In what follows, we denote by  $C_\Pi$  with  $\Pi \subset \{\gamma, \nu, \Xi, \varsigma\}$  a constant that depends on the parameters included in  $\Pi$  which may vary from one occasion to another.

**Lemma C.3.** Suppose that Condition 1 holds.

(i) Under Condition 1 (a), we have  $\sup_{\mathbf{a}, \mathbf{b} \in \mathbb{B}_2(1)} \|W_t(\mathbf{a}, \mathbf{b})\|_{\psi_\kappa} \leq C_{\gamma, \Xi, \varsigma} C_\xi^2 < \infty$  with  $\kappa = 2\gamma + 1$ .

(ii) Under Condition 1 (b), we have  $\sup_{\mathbf{a} \in \mathbb{B}_2(1)} \|U_t(\mathbf{a})\|_2 \leq C_{\Xi, \varsigma}$ .

*Proof.* In what follows, we denote by  $\mu_\nu = \|\xi_{it}\|_\nu$ . For given  $\nu > 1$ , we have

$$\sup_{\mathbf{a} \in \mathbb{B}_2(1)} \delta_{t, \nu}(\mathbf{a}) = \left\| \mathbf{a}^\top \mathbf{D}_t(\xi_0 - \xi'_0) \right\|_\nu \leq C_\nu \mu_\nu \sqrt{2 \sup_{\mathbf{a} \in \mathbb{B}_2(1)} |\mathbf{a}^\top \mathbf{D}_t|_2^2} \leq C_\nu \mu_\nu \Xi(1+t)^{-\varsigma} \quad (\text{C.16})$$

with  $C_\nu = \max(1/(\nu-1), \sqrt{\nu-1})$ , where the inequality follows from Lemma 2 of Chen et al. (2021) (Burkholder's inequality) and Minkowski inequality, and the second from Condition 1 and from that  $\|\mathbf{D}_t\|_2 \leq \sqrt{\|\mathbf{D}_t\|_1 \|\mathbf{D}_t\|_\infty}$  (with  $\|\cdot\|_a$  denoting the induced matrix norms). Therefore, under Condition 1 (b),

$$\sup_{\mathbf{a} \in \mathbb{B}_2(1)} \|U_t(\mathbf{a})\|_2 \leq \Xi \sum_{t=0}^{\infty} (1+t)^{-\varsigma} \leq C_{\Xi, \varsigma},$$

which proves (ii). Note that by Hölder and Minkowski's inequalities,

$$\begin{aligned} \delta_{t, \nu}(\mathbf{a}, \mathbf{b}) &\leq \left\| \sum_{\ell=0}^{\infty} \mathbf{a}^\top \mathbf{D}_\ell \xi_{t-\ell} \right\|_{2\nu} \left\| \mathbf{b}^\top \mathbf{D}_t(\xi_0 - \xi'_0) \right\|_{2\nu} \\ &\quad + \left\| \sum_{\ell=0, \ell \neq t}^{\infty} \mathbf{b}^\top \mathbf{D}_\ell \xi_{t-\ell} + \mathbf{b}^\top \mathbf{D}_t \xi'_0 \right\|_{2\nu} \left\| \mathbf{a}^\top \mathbf{D}_t(\xi_0 - \xi'_0) \right\|_{2\nu}. \end{aligned}$$

For given  $\nu > 2$ , similarly as in (C.16), we can show that

$$\begin{aligned} \sup_{\mathbf{a} \in \mathbb{B}_2(1)} \left\| \sum_{\ell=0}^{\infty} \mathbf{a}^\top \mathbf{D}_\ell \xi_{t-\ell} \right\|_{2\nu} &\leq \sum_{\ell=0}^{\infty} \sup_{\mathbf{a} \in \mathbb{B}_2(1)} \left\| \mathbf{a}^\top \mathbf{D}_\ell \xi_{t-\ell} \right\|_{2\nu} \\ &\leq C_{2\nu} \mu_{2\nu} \sum_{\ell=0}^{\infty} \sqrt{\sup_{\mathbf{a} \in \mathbb{B}_2(1)} |\mathbf{a}^\top \mathbf{D}_\ell|_2^2} \leq C_{2\nu} \mu_{2\nu} \sum_{\ell=0}^{\infty} \Xi(1+\ell)^{-\varsigma} \leq C_{\gamma, \Xi, \varsigma} C_\xi^2 \nu^{\gamma+1/2} \end{aligned} \quad (\text{C.17})$$

under Condition 1 (a). Then, (C.16)–(C.17) lead to

$$\begin{aligned} \sup_{\mathbf{a}, \mathbf{b} \in \mathbb{B}_2(1)} \delta_{t, \nu}(\mathbf{a}, \mathbf{b}) &\leq C_{\gamma, \Xi, \varsigma} C_\xi^2 \nu^{2\gamma+1} (1+t)^{-\varsigma}, \quad \text{and} \\ \sup_{\mathbf{a}, \mathbf{b} \in \mathbb{B}_2(1)} \|W_t(\mathbf{a}, \mathbf{b})\|_\nu &\leq C_{\gamma, \Xi, \varsigma} C_\xi^2 \nu^{2\gamma+1} \sum_{t=0}^{\infty} (1+t)^{-\varsigma} \leq C_{\gamma, \Xi, \varsigma} C_\xi^2 \nu^{2\gamma+1}, \end{aligned}$$

such that we have  $\sup_{\mathbf{a}, \mathbf{b} \in \mathbb{B}_2(1)} \|W(\mathbf{a}, \mathbf{b})\|_{\psi_\kappa} \leq C_{\gamma, \Xi, \varsigma} C_\xi^2$  with  $\kappa = 2\gamma + 1$ , which proves (i).  $\square$

**Lemma C.4.** Under Condition 1 (a), there exist fixed constants  $C', C'' > 0$  such that for all  $0 \leq s < e \leq n$  and  $z > 0$ , we have

$$\sup_{\mathbf{a}, \mathbf{b} \in \mathbb{B}_2(1)} \mathbb{P} \left( \frac{1}{\sqrt{e-s}} \left| \sum_{t=s+1}^e \mathbf{a}^\top \mathbf{Z}_t \mathbf{Z}_t^\top \mathbf{b} - \mathbb{E} \left( \sum_{t=s+1}^e \mathbf{a}^\top \mathbf{Z}_t \mathbf{Z}_t^\top \mathbf{b} \right) \right| \geq z \right) \leq C' \exp \left( -C'' z^{\frac{2}{4\gamma+3}} \right).$$

*Proof.* By Lemma C.3 (i) and Lemma C.4 of Zhang and Wu (2017), there exist constants  $C', C'' > 0$  that depend on  $\gamma, \Xi, \varsigma$  and  $C_\xi$ , such that for all  $z > 0$ ,

$$\begin{aligned} & \sup_{\mathbf{a}, \mathbf{b} \in \mathbb{B}_2(1)} \mathbb{P} \left( \frac{1}{\sqrt{e-s}} \left| \sum_{t=s+1}^e \mathbf{a}^\top \mathbf{Z}_t \mathbf{Z}_t^\top \mathbf{b} - \mathbb{E} \left( \sum_{t=s+1}^e \mathbf{a}^\top \mathbf{Z}_t \mathbf{Z}_t^\top \mathbf{b} \right) \right| \geq z \right) \\ & \leq C' \exp \left( -\frac{(4\gamma+3)z^{\frac{2}{4\gamma+3}}}{4e(C_{\gamma, \Xi, \varsigma} C_\xi^2)^{\frac{2}{4\gamma+3}}} \right) \leq C' \exp \left( -C'' z^{\frac{2}{4\gamma+3}} \right). \end{aligned}$$

$\square$

**Lemma C.5.** Under Condition 1 (b), there exists a fixed constants  $C''' > 0$  such that for all  $0 \leq s < e \leq n$  and  $0 < z < C_{\Xi, \varsigma}^2 \sqrt{e-s}$ , we have

$$\sup_{\mathbf{a}, \mathbf{b} \in \mathbb{B}_2(1)} \mathbb{P} \left( \frac{1}{\sqrt{e-s}} \left| \sum_{t=s+1}^e \mathbf{a}^\top \mathbf{Z}_t \mathbf{Z}_t^\top \mathbf{b} - \mathbb{E} \left( \sum_{t=s+1}^e \mathbf{a}^\top \mathbf{Z}_t \mathbf{Z}_t^\top \mathbf{b} \right) \right| \geq z \right) \leq 6 \exp(-C''' z^2).$$

*Proof.* By Lemma C.3 (ii) and Theorem 6.6 of Zhang and Wu (2021), there exists an absolute constant  $C > 0$  such that for all  $0 < z < C_{\Xi, \varsigma}^2 \sqrt{e-s}$ ,

$$\begin{aligned} & \sup_{\mathbf{a} \in \mathbb{B}_2(1)} \mathbb{P} \left( \frac{1}{\sqrt{e-s}} \left| \sum_{t=s+1}^e \mathbf{a}^\top \mathbf{Z}_t \mathbf{Z}_t^\top \mathbf{a} - \mathbb{E} \left( \sum_{t=s+1}^e \mathbf{a}^\top \mathbf{Z}_t \mathbf{Z}_t^\top \mathbf{a} \right) \right| \geq z \right) \\ & \leq 2 \exp \left[ -C \min \left( \frac{z^2}{C_{\Xi, \varsigma}^4}, \frac{z\sqrt{e-s}}{C_{\Xi, \varsigma}^2} \right) \right] \leq 2 \exp(-CC_{\Xi, \varsigma}^{-4} z^2). \end{aligned}$$

Then noting that

$$\begin{aligned} & \sup_{\mathbf{a}, \mathbf{b} \in \mathbb{B}_2(1)} \mathbb{P} \left( \frac{2}{\sqrt{e-s}} \left| \sum_{t=s+1}^e \mathbf{a}^\top \mathbf{Z}_t \mathbf{Z}_t^\top \mathbf{b} - \mathbb{E} \left( \sum_{t=s+1}^e \mathbf{a}^\top \mathbf{Z}_t \mathbf{Z}_t^\top \mathbf{b} \right) \right| \geq z \right) \leq \\ & \sup_{\mathbf{a}, \mathbf{b} \in \mathbb{B}_2(1)} \mathbb{P} \left( \frac{1}{\sqrt{e-s}} \left| \sum_{t=s+1}^e (\mathbf{a} + \mathbf{b})^\top \mathbf{Z}_t \mathbf{Z}_t^\top (\mathbf{a} + \mathbf{b}) - \mathbb{E} \left( \sum_{t=s+1}^e (\mathbf{a} + \mathbf{b})^\top \mathbf{Z}_t \mathbf{Z}_t^\top (\mathbf{a} + \mathbf{b}) \right) \right| \geq \frac{z}{3} \right) \\ & + 2 \sup_{\mathbf{a} \in \mathbb{B}_2(1)} \mathbb{P} \left( \frac{1}{\sqrt{e-s}} \left| \sum_{t=s+1}^e \mathbf{a}^\top \mathbf{Z}_t \mathbf{Z}_t^\top \mathbf{a} - \mathbb{E} \left( \sum_{t=s+1}^e \mathbf{a}^\top \mathbf{Z}_t \mathbf{Z}_t^\top \mathbf{a} \right) \right| \geq \frac{z}{3} \right) \leq 6 \exp \left( -\frac{Cz^2}{9C_{\Xi, \varsigma}^4} \right), \end{aligned}$$

we can find  $C'''$  that depends on  $\Xi$  and  $\varsigma$ .  $\square$

### C.2.2 Proof of Proposition 2 (i)

Recalling  $C'$  from Lemma C.4, we set  $c_1 = 3C'$ .

*Verification of Assumption 2:*

By assumption, we have  $\mathbf{E}(\mathbf{x}_t \varepsilon_t) = \mathbf{0}$ . Then setting  $\mathbf{a} = \mathbf{e}_i$ ,  $i = 1, \dots, p$ ,  $\mathbf{b} = \mathbf{e}_{p+1}$  and  $z = C_{\text{DEV}} \log^{2\gamma+3/2}(p \vee n)$  in Lemma C.4,

$$\mathbf{P}(\mathcal{D}^{(1)}) \geq 1 - C' p n^2 \exp \left( -C'' C_{\text{DEV}}^{\frac{2}{4\gamma+3}} \log(p \vee n) \right). \quad (\text{C.18})$$

Next, by construction,

$$\sum_{t=s+1}^e (\boldsymbol{\beta}(t) - \boldsymbol{\beta}_{s,e}^*) = \mathbf{0} \quad \text{and} \quad \max_{\substack{0 \leq s < e \leq n \\ |\{s+1, \dots, e\} \cap \Theta| \leq 1}} \max_{s < t \leq e} \|\boldsymbol{\beta}(t) - \boldsymbol{\beta}_{s,e}^*\|_2 \leq C_\delta \quad (\text{C.19})$$

under Assumption 4, and

$$\mathbf{E} \left[ \sum_{t=s+1}^e \mathbf{x}_t \mathbf{x}_t^\top (\boldsymbol{\beta}(t) - \boldsymbol{\beta}_{s,e}^*) \right] = \boldsymbol{\Sigma}_x \sum_{t=s+1}^e (\boldsymbol{\beta}(t) - \boldsymbol{\beta}_{s,e}^*) = \mathbf{0} \quad (\text{C.20})$$

under Assumption 1. Then setting  $\mathbf{a} = \mathbf{e}_i$ ,  $i = 1, \dots, p$ ,  $\mathbf{b} = \boldsymbol{\beta}(t) - \boldsymbol{\beta}_{s,e}^*$  for given  $s, e$  and  $t \in \{s+1, \dots, e\}$  and  $z = C_{\text{DEV}} C_\delta \log^{2\gamma+3/2}(p \vee n)$  in Lemma C.4,

$$\mathbf{P}(\mathcal{D}^{(2)}) \geq 1 - C' p n^3 \exp \left( -C'' (C_{\text{DEV}} C_\delta)^{\frac{2}{4\gamma+3}} \log(p \vee n) \right), \quad (\text{C.21})$$

from (C.19) and (C.20). Combining (C.18) and (C.21), we can find large enough  $C_{\text{DEV}}$  that depends only on  $C''$ ,  $\gamma$ ,  $C_\delta$  and  $c_2$  such that  $\mathbf{P}(\mathcal{D}^{(1)} \cap \mathcal{D}^{(2)}) \geq 1 - 2c_1(p \vee n)^{-c_2}/3$ .

*Verification of Assumption 3:*

Let  $b_{s,e}$  denote an integer that depends on  $(e-s)$  for some  $0 \leq s < e \leq n$ , and define

$$\mathcal{R} = \left\{ \sup_{\mathbf{a} \in \mathbb{K}(2b_{s,e})} \frac{1}{e-s} \left| \sum_{t=s+1}^e \mathbf{a}^\top (\mathbf{x}_t \mathbf{x}_t^\top - \boldsymbol{\Sigma}_x) \mathbf{a} \right| \geq \frac{\Lambda_{\min}(\boldsymbol{\Sigma}_x)}{54} \text{ for all } 0 \leq s < e \leq n \right. \\ \left. \text{with } e-s \geq C_0 \log^{4\gamma+3}(p \vee n) \text{ and } |\{s+1, \dots, e\} \cap \Theta| \leq 1 \right\}.$$

By Lemma C.4 and Lemma F.2 of Basu and Michailidis (2015), we have

$$\mathbf{P}(\mathcal{R}^c) \leq \sum_{\substack{0 \leq s < e \leq n \\ e-s \geq C_0 \log^{4\gamma+3}(p \vee n) \\ |\{s+1, \dots, e\} \cap \Theta| \leq 1}} C' \exp \left[ -C'' \left( \frac{\sqrt{e-s} \Lambda_{\min}(\boldsymbol{\Sigma}_x)}{54} \right)^{\frac{2}{4\gamma+3}} + 2b_{s,e} \log(p) \right]$$

$$\leq C' n^2 \exp \left[ -\frac{C''}{2} \left( \frac{C_0^{1/2} \Lambda_{\min}(\mathbf{\Sigma}_x)}{54} \right)^{\frac{2}{4\gamma+3}} \log(p \vee n) \right],$$

where the last inequality follows with

$$b_{s,e} = \left\lfloor \frac{C''}{4 \log(p)} \left( \frac{\sqrt{e-s} \Lambda_{\min}(\mathbf{\Sigma}_x)}{54} \right)^{\frac{2}{4\gamma+3}} \right\rfloor,$$

which satisfies  $b_{s,e} \geq 1$  for large enough  $C_0$ . Further, we can find  $C_0$  that depends only on  $C''$ ,  $\Lambda_{\min}(\mathbf{\Sigma}_x)$ ,  $\gamma$  and  $c_2$  which leads to  $\mathbf{P}(\mathcal{R}) \geq 1 - c_1(p \vee n)^{-c_2}/3$ . Then, by Lemma 12 of Loh and Wainwright (2012), on  $\mathcal{R}$ , we have

$$\begin{aligned} \sum_{t=s+1}^e \mathbf{a}^\top \mathbf{x}_t \mathbf{x}_t^\top \mathbf{a} &\geq \Lambda_{\min}(\mathbf{\Sigma}_x)(e-s) |\mathbf{a}|_2^2 \\ &\quad - \frac{\Lambda_{\min}(\mathbf{\Sigma}_x)}{2}(e-s) \left( |\mathbf{a}|_2^2 + \frac{4 \log(p)}{C''} \left( \frac{54}{\sqrt{e-s} \Lambda_{\min}(\mathbf{\Sigma}_x)} \right)^{\frac{2}{4\gamma+3}} |\mathbf{a}|_1^2 \right) \\ &\geq \omega(e-s) |\mathbf{a}|_2^2 - C_{\text{RSC}} \log(p)(e-s)^{\frac{4\gamma+2}{4\gamma+3}} |\mathbf{a}|_1^2 \end{aligned}$$

for all  $\mathbf{a} \in \mathbb{R}^p$ , with  $\omega = \Lambda_{\min}(\mathbf{\Sigma}_x)/2$  and  $C_{\text{RSC}}$  depending only on  $C''$ ,  $\gamma$  and  $\Lambda_{\min}(\mathbf{\Sigma}_x)$ . Analogously we have on  $\mathcal{R}$ ,

$$\sum_{t=s+1}^e \mathbf{a}^\top \mathbf{x}_t \mathbf{x}_t^\top \mathbf{a} \leq \bar{\omega}(e-s) |\mathbf{a}|_2^2 + C_{\text{RSC}} \log(p)(e-s)^{\frac{4\gamma+2}{4\gamma+3}} |\mathbf{a}|_1^2$$

for all  $\mathbf{a} \in \mathbb{R}^p$ , with  $\bar{\omega} = 3\Lambda_{\max}(\mathbf{\Sigma}_x)/2$ .

Combining the arguments above, we have  $\mathbf{P}(\mathcal{D}^{(1)} \cap \mathcal{D}^{(2)} \cap \mathcal{R}^{(1)} \cap \mathcal{R}^{(2)}) \geq 1 - c_1(p \vee n)^{-c_2}$ , with  $\tau = (4\gamma + 2)/(4\gamma + 3)$  and  $\rho_{n,p} = \log^{2\gamma+3/2}(p \vee n)$ .

### C.2.3 Proof of Proposition 2 (ii)

We set  $c_1 = 18$ .

*Verification of Assumption 2:*

By assumption, we have  $\mathbf{E}(\mathbf{x}_t \varepsilon_t) = \mathbf{0}$ . Then setting  $\mathbf{a} = \mathbf{e}_i$ ,  $i = 1, \dots, p$ ,  $\mathbf{b} = \mathbf{e}_{p+1}$  and  $z = C_{\text{DEV}} \sqrt{\log(p \vee n)}$  in Lemma C.5,

$$\mathbf{P}(\mathcal{D}^{(1)}) \geq 1 - 6pn^2 \exp \left( -C''' C_{\text{DEV}}^2 \log(p \vee n) \right), \quad (\text{C.22})$$

provided that  $C_0 > C_{\Xi, \varsigma}^{-4} C_{\text{DEV}}^2$ . Also, setting  $\mathbf{a} = \mathbf{e}_i$ ,  $i = 1, \dots, p$ ,  $\mathbf{b} = \boldsymbol{\beta}(t) - \boldsymbol{\beta}_{s,e}^*$  for given  $s, e$  and  $t \in \{s+1, \dots, e\}$  and  $z = C_{\text{DEV}} C_\delta \sqrt{\log(p \vee n)}$  in Lemma C.5,

$$\mathbf{P}(\mathcal{D}^{(2)}) \geq 1 - 6pn^3 \exp \left( -C''' C_{\text{DEV}}^2 C_\delta^2 \log(p \vee n) \right), \quad (\text{C.23})$$

from (C.19) and (C.20). Combining (C.22) and (C.23), we can find large enough  $C_{\text{DEV}}$  that depends only on  $C'''$ ,  $C_\delta$  and  $c_2$  such that  $\mathbf{P}(\mathcal{D}^{(1)} \cap \mathcal{D}^{(2)}) \geq 1 - 2c_1(p \vee n)^{-c_2}/3$ .

*Verification of Assumption 3:*

Let  $b_{s,e}$  denote an integer that depends on  $(e - s)$  for some  $0 \leq s < e \leq n$ , and define

$$\mathcal{R} = \left\{ \sup_{\mathbf{a} \in \mathbb{K}(2b_{s,e})} \frac{1}{e-s} \left| \sum_{t=s+1}^e \mathbf{a}^\top (\mathbf{x}_t \mathbf{x}_t^\top - \boldsymbol{\Sigma}_x) \mathbf{a} \right| \geq \frac{\Lambda_{\min}(\boldsymbol{\Sigma}_x)}{54} \text{ for all } 0 \leq s < e \leq n \right. \\ \left. \text{with } e-s \geq C_0 \log(p \vee n) \text{ and } |\{s+1, \dots, e\} \cap \Theta| \leq 1 \right\}.$$

Then by Lemma C.5 and Lemma F.2 of Basu and Michailidis (2015), we have

$$\mathbf{P}(\mathcal{R}^c) \leq \sum_{\substack{0 \leq s < e \leq n \\ e-s \geq C_0 \log(p \vee n) \\ |\{s+1, \dots, e\} \cap \Theta| \leq 1}} 6 \exp \left[ -C'''(e-s) \left( \frac{\Lambda_{\min}(\boldsymbol{\Sigma}_x)}{54} \right)^2 + 2b_{s,e} \log(p) \right] \\ \leq 6n^2 \exp \left[ -\frac{C'''C_0}{2} \left( \frac{\Lambda_{\min}(\boldsymbol{\Sigma}_x)}{54} \right)^2 \log(p \vee n) \right],$$

where the last inequality follows with

$$b_{s,e} = \left\lceil \frac{C'''(e-s)}{4 \log(p)} \left( \frac{\Lambda_{\min}(\boldsymbol{\Sigma}_x)}{54} \right)^2 \right\rceil,$$

which satisfies  $b_{s,e} \geq 1$  for large enough  $C_0$ . Further, we can find  $C_0$  that depends only on  $C'''$ ,  $\Lambda_{\min}(\boldsymbol{\Sigma}_x)$  and  $c_2$  which leads to  $\mathbf{P}(\mathcal{R}) \geq 1 - c_1(p \vee n)^{-c_2}/3$ . Then, by Lemma 12 of Loh and Wainwright (2012), on  $\mathcal{R}$ , we have

$$\sum_{t=s+1}^e \mathbf{a}^\top \mathbf{x}_t \mathbf{x}_t^\top \mathbf{a} \geq \Lambda_{\min}(\boldsymbol{\Sigma}_x)(e-s)|\mathbf{a}|_2^2 \\ - \frac{\Lambda_{\min}(\boldsymbol{\Sigma}_x)}{2}(e-s) \left( |\mathbf{a}|_2^2 + \frac{4 \log(p)}{C'''(e-s)} \left( \frac{54}{\Lambda_{\min}(\boldsymbol{\Sigma}_x)} \right)^2 |\mathbf{a}|_1^2 \right) \\ \geq \omega(e-s)|\mathbf{a}|_2^2 - C_{\text{RSC}} \log(p) |\mathbf{a}|_1^2$$

for all  $\mathbf{a} \in \mathbb{R}^p$ , with  $\omega = \Lambda_{\min}(\boldsymbol{\Sigma}_x)/2$  and  $C_{\text{RSC}}$  depending only on  $C'''$  and  $\Lambda_{\min}(\boldsymbol{\Sigma}_x)$ . Analogously we have on  $\mathcal{R}$ ,

$$\sum_{t=s+1}^e \mathbf{a}^\top \mathbf{x}_t \mathbf{x}_t^\top \mathbf{a} \leq \bar{\omega}(e-s)|\mathbf{a}|_2^2 + C_{\text{RSC}} \log(p) |\mathbf{a}|_1^2$$

for all  $\mathbf{a} \in \mathbb{R}^p$ , with  $\bar{\omega} = 3\Lambda_{\max}(\boldsymbol{\Sigma}_x)/2$ .

Combining the arguments above, we have  $\mathbf{P}(\mathcal{D}^{(1)} \cap \mathcal{D}^{(2)} \cap \mathcal{R}^{(1)} \cap \mathcal{R}^{(2)}) \geq 1 - c_1(p \vee n)^{-c_2}$ , with

$\tau = 0$  and  $\rho_{n,p} = \sqrt{\log(p \vee n)}$ .

### C.3 Proof of Theorem 4

In what follows, we operate on  $\mathcal{M} = \mathcal{D}^{(1)} \cap \mathcal{D}^{(2)} \cap \mathcal{R}^{(1)} \cap \mathcal{R}^{(2)} \cap \mathcal{B}$ . Under Assumption 5', we have all  $G \in \mathcal{G}$  satisfy  $G \geq C_0 \max\{\rho_{n,p}^2, (\omega^{-1} \mathfrak{s} \log(p))^{1/(1-\tau)}\}$  such that the lower bound on  $(e - s)$  made in  $\mathcal{B}$  (see Lemma C.2) is met by all  $s = k$  and  $e = k + G$ ,  $k = 0, \dots, n - G$ .

For some  $k$  and  $G \in \mathcal{G}$ , we write  $\mathcal{I}(k, G) = \{k - G + 1, \dots, k + G\}$ . Recall that for each pre-estimator  $\tilde{\theta} \in \tilde{\Theta}(G)$ , we denote by  $\mathcal{I}(\tilde{\theta}) = \mathcal{I}(\tilde{\theta}, G)$  its detection interval. By the same arguments adopted in (C.4) and Lemmas C.1 and C.2, we have

$$\max_{G \in \mathcal{G}} \max_{\substack{G \leq k \leq n-G \\ |\mathcal{I}(k, G) \cap \Theta| \leq 1}} |T_k(G) - T_k^*(G)| \leq \frac{24\sqrt{\mathfrak{s}}\lambda}{\omega} \quad \text{and} \quad T_k^*(G) = 0 \quad \text{if} \quad \mathcal{I}(k, G) \cap \Theta = \emptyset. \quad (\text{C.24})$$

Then, we make the following observations.

- (i) From (C.24) and the requirement on  $D$  in (18), we have  $\mathcal{I}(\tilde{\theta}) \cap \Theta \neq \emptyset$  for all  $\tilde{\theta} \in \tilde{\Theta}(\mathcal{G})$ , i.e. each pre-estimator in  $\tilde{\Theta}(\mathcal{G})$  has (at least) one change point in its detection interval.
- (ii) Under Assumption 5', for each  $\theta_j$ ,  $j = 1, \dots, q$ , there exists one pre-estimator  $\tilde{\theta} \in \tilde{\Theta}(G_{(j)})$  such that  $\mathcal{I}(\tilde{\theta}) \cap \Theta = \{\theta_j\}$  and  $|\tilde{\theta} - \theta_j| < \lfloor G_{(j)}/2 \rfloor$ , by the arguments used in the proof of Theorem 1 (i).

Thanks to (ii), there exists an anchor estimator  $\tilde{\theta}^A \in \tilde{\Theta}^A$  for each  $\theta_j$ , in the sense that  $\theta_j \in \mathcal{I}(\tilde{\theta}^A)$  and further, this anchor estimator  $\tilde{\theta}^A$  is detected with some bandwidth  $G \leq G_{(j)}$ . At the same time, there is at most a single anchor estimator  $\tilde{\theta}^A$  fulfilling  $\theta_j \in \mathcal{I}(\tilde{\theta}^A)$  by its construction in (14), and (i) ensures that all anchor estimators contain one change point in its detection interval. Therefore, we have  $\hat{q} = |\tilde{\Theta}^A| = q$  and we may write  $\tilde{\Theta}^A = \{\tilde{\theta}_j^A, 1 \leq j \leq q : \tilde{\theta}_1^A < \dots < \tilde{\theta}_q^A\}$ .

Next, by (ii), there exists some  $\tilde{\theta} \in \tilde{\Theta}(G_{(j)})$  fulfilling (15) for each  $j = 1, \dots, q$ . To see this, note that if  $\tilde{\theta} \in \tilde{\Theta}(G_{(j)})$  detects  $\theta_j$  in the sense that  $\theta_j \in \mathcal{I}(\tilde{\theta})$ ,

$$\left\{ \tilde{\theta} - G_{(j)} - \left\lfloor \frac{G_{(j)}}{2} \right\rfloor + 1, \dots, \tilde{\theta} + G_{(j)} + \left\lfloor \frac{G_{(j)}}{2} \right\rfloor \right\} \subset \{\theta_j - 2G_{(j)} + 1, \theta_j + 2G_{(j)}\}, \quad \text{while}$$

$$\mathcal{I}(\tilde{\theta}_{j-1}^A) \subset \{\theta_{j-1} - 2G_{(j-1)} + 1, \dots, \theta_{j-1} + 2G_{(j-1)}\} \quad \text{and}$$

$$\mathcal{I}(\tilde{\theta}_{j+1}^A) \subset \{\theta_{j+1} - 2G_{(j+1)} + 1, \dots, \theta_{j+1} + 2G_{(j+1)}\},$$

and the sets on RHS do not overlap under Assumption 5' (a). This in turn implies that we have  $|\mathcal{C}_j| \geq 1$ . Also for  $\tilde{\theta}_j^M \in \mathcal{C}_j$ , we have that its detection bandwidth  $G_j^M$  satisfies

$$\frac{3}{2} G_j^M \leq \min(\theta_{j+1} - \theta_j, \theta_j - \theta_{j-1}) \quad \text{and} \quad G_j^M \geq G_{(j)}$$



by the construction of  $\mathcal{C}_j$ . Also, the bandwidths generated as in Remark 2 satisfy

$$G_{\ell-1} + \frac{1}{2}G_{\ell-1} \leq G_{\ell-1} + G_{\ell-2} = G_\ell \leq 2G_{\ell-1}, \quad \text{such that} \quad \frac{1}{2}G_\ell \leq G_{\ell-1} \leq \frac{2}{3}G_\ell \text{ for } \ell \geq 2,$$

and therefore

$$\frac{1}{4}G_{(j)} \leq G_j^* \quad \text{and} \quad G_j^* \leq \left(\frac{3}{4} \cdot \frac{2}{3} + \frac{1}{4}\right) G_j^M \leq \frac{1}{2} \min(\theta_{j+1} - \theta_j, \theta_j - \theta_{j-1}). \quad (\text{C.25})$$

Further, by that  $|\tilde{\theta}_j^m - \theta_j| < G_j^m$  (see (i)) and

$$2G_j^m + G_j^* = \frac{11}{4}G_j^m + \frac{1}{4}G_j^M \leq \frac{11}{4}G_{(j)} + \frac{1}{4}G_j^M \leq \frac{41}{48} \min(\theta_{j+1} - \theta_j, \theta_j - \theta_{j-1}),$$

we have

$$\{\tilde{\theta}_j^m - G_j^m - G_j^* + 1, \dots, \tilde{\theta}_j^m - G_j^m\} \cap \{\tilde{\theta}_j^m + G_j^m + 1, \dots, \tilde{\theta}_j^m + G_j^m + G_j^*\} \cap \Theta = \emptyset. \quad (\text{C.26})$$

From (C.25) and Assumption 5' (b), we have

$$\delta_j^2 G_j^* \geq C_1 \max \left\{ \omega^{-2} \mathfrak{s} \rho_{n,p}^2, (\omega^{-1} \mathfrak{s} \log(p))^{1/(1-\tau)} \right\}$$

and from (C.26) and Lemma C.2, we have  $\Delta_j^L = \hat{\beta}_j^L - \beta_{j-1}$  and  $\Delta_j^R = \hat{\beta}_j^R - \beta_j$  satisfy

$$\begin{aligned} \max \left( |\Delta_j^L|_2, |\Delta_j^R|_2 \right) &\leq \frac{12\sqrt{2\mathfrak{s}\lambda}}{\omega\sqrt{G_j^*}} \leq \frac{24\sqrt{2\mathfrak{s}\lambda}}{\omega\sqrt{G_{(j)}}}, \\ |\Delta_j^L(\mathcal{S}_{j-1}^c)|_1 &\leq 3|\Delta_j^L(\mathcal{S}_{j-1})|_1 \quad \text{and} \quad |\Delta_j^R(\mathcal{S}_j^c)|_1 \leq 3|\Delta_j^R(\mathcal{S}_j)|_1, \end{aligned}$$

such that the arguments analogous to those employed in the proof of Theorem 1 (ii) are applicable to establish the localisation rate of  $\tilde{\theta}_j$ , which completes the proof.

## D Algorithms

## E Further information on the real datasets

Tables E.1–E.2 list the covariates included in the datasets analysed in Section 5.

---

**Algorithm 1:** MOSEG: Single-bandwidth two-stage data segmentation methodology under a regression model.

---

**input** : Bandwidth  $G$ , grid resolution  $r$ , penalty  $\lambda$ , threshold  $D$ ,  $\eta \in (0, 1]$   
**initialise:**  $\tilde{\Theta} = \emptyset$ ,  $\hat{\Theta} = \emptyset$   
// Stage 1  
Compute  $T_k(G)$  in (2) for all  $k \in \mathcal{T} = \mathcal{T}(r, G)$   
Add all  $\tilde{\theta}$  satisfying  $T_{\tilde{\theta}}(G) > D$  and  $\tilde{\theta} = \arg \min_{k \in \{\tilde{\theta} - \lfloor \eta G \rfloor + 1, \dots, \tilde{\theta} + \lfloor \eta G \rfloor\} \cap \mathcal{T}} T_k(G)$  to  $\tilde{\Theta}$ ,  
and set  $\tilde{\Theta} = \{\tilde{\theta}_j, 1 \leq j \leq \hat{q}\}$   
// Stage 2  
**for**  $j = 1, \dots, \hat{q}$  **do**  
    Identify  $\hat{\theta}_j = \arg \min_{\tilde{\theta}_j - G + 1 \leq j \leq \tilde{\theta}_j + G} Q(k; \tilde{\theta}_j - G, \tilde{\theta}_j + G, \hat{\beta}_j^L, \hat{\beta}_j^R)$  with  $\hat{\beta}_j^L$  and  $\hat{\beta}_j^R$   
    computed as in (8), and add it to  $\hat{\Theta}$   
**end**  
**return**  $\hat{\Theta}$

---



---

**Algorithm 2:** MOSEG.MS: Multiscale extension of MOSEG.

---

**input** : A set of bandwidths  $\mathcal{G}$ , grid resolution  $r$ , penalty  $\lambda$ , threshold  $D$ ,  $\eta \in (0, 1]$   
**initialise:**  $\tilde{\Theta}^A = \emptyset$ ,  $\tilde{\Theta} = \emptyset$ ,  $\mathcal{C}_j = \emptyset$  for all  $j$   
// Pre-estimator generation  
**for**  $h = 1, \dots, H$  **do**  
    Initialise  $\tilde{\Theta}(G_h) = \emptyset$   
    Compute  $T_k(G_h)$  in (2) for all  $k \in \mathcal{T}_h = \mathcal{T}(r, G_h)$   
    Add all  $\tilde{\theta}$  satisfying  $T_{\tilde{\theta}}(G_h) > D$  and  $\tilde{\theta} = \arg \min_{k \in \mathcal{I}_\eta(\tilde{\theta}) \cap \mathcal{T}_h} T_k(G_h)$ , to  $\tilde{\Theta}(G_h)$   
**end**  
// Anchor change point estimator identification  
Identify all  $\tilde{\theta}(G) \in \cup_{h=1}^H \tilde{\Theta}(G_h)$  satisfying (14), and add all such estimators to  $\tilde{\Theta}^A$ ,  
which is denoted by  $\tilde{\Theta}^A = \{\tilde{\theta}_j^A, 1 \leq j \leq \hat{q}: \tilde{\theta}_1^A < \dots < \tilde{\theta}_{\hat{q}}^A\}$   
**for**  $j = 1, \dots, \hat{q}$  **do**  
    // Pre-estimator clustering  
    Identify all  $\tilde{\theta} \in \cup_{h=1}^H \tilde{\Theta}(G_h)$  satisfying (15) and add it to  $\mathcal{C}_j$   
    // Location refinement  
    Add  $\check{\theta}_j$  obtained as in (16) to  $\hat{\Theta}$   
**end**  
**return**  $\check{\Theta}$

---

Table E.1: Covariates contained in the sea ice extent dataset analysed in Section 5.1 (cf. Coulombe and Göbel (2021), Table 1)

Name	Description
Age_withland	Gridded monthly mean of sea ice age (with land)
Age_wo_land	Gridded monthly mean of sea ice age (without land)
AT	Gridded monthly mean of air temperature
Albedo	Gridded monthly mean of surface albedo
CO <sub>2</sub>	Global monthly mean of CO <sub>2</sub>
EMIS	Gridded monthly mean of surface emissivity
LWGAB	Gridded monthly mean of surface absorbed longwave radiation
LWGEM	Gridded monthly mean of longwave flux emitted from surface
LWGNT	Gridded monthly mean of surface net downward longwave flux
LWTUP	Gridded monthly mean of upwelling longwave flux at TOA
PR	Gridded monthly mean of precipitation
SST	Median Northern Hemisphere mean sea surface temperature anomaly (relative to 1961–90)
SWGNT	Gridded monthly mean of surface net downward shortwave flux
SWTNT	Gridded monthly mean of TOA net downward shortwave flux
TAUTOT	Gridded monthly mean of in-cloud optical SIT of all clouds
SIT	Gridded monthly mean of sea ice thickness
TCC	Gridded monthly mean of total cloud cover
TS	Gridded monthly mean of surface skin temperature

Table E.2: Covariates contained in the equity premium dataset analysed in Section 5.2 (cf. Koo et al. (2020), Table 3)

Name	Description
d/p	Dividend price ratio: difference between the log of dividends and the log of prices
d/y	Dividend yield: difference between the log of dividends and the log of lagged prices
e/p	Earnings price ratio: difference between the log of earnings and the log of prices
d/e	Dividend payout ratio: difference between the log of dividends and the log of earnings
b/m	Book-to-market ratio: ratio of book value to market value for the Dow Jones Industrial Average
ntis	Net equity expansion: ratio of 12-month moving sums of net issues by NYSE listed stocks over the total end-of-year market capitalization of NYSE stocks
tbl	Treasury bill rates: 3-month Treasury bill rates
lty	Long-term yield: long-term government bond yield
tms	Term spread: difference between the long term bond yield and the Treasury bill rate
dfy	Default yield spread: difference between Moody’s BAA and AAA-rated corporate bond yields
dfr	Default return spread: difference between the returns of long-term corporate and government bonds
svar	Log of stock variance obtained as the sum of squared daily returns on S&P500 index
infl	Inflation: CPI inflation for all urban consumers
ltr	Long-term return: return of long term government bonds